RSL24D1 sustains steady-state ribosome biogenesis and pluripotency translational programs in embryonic stem cells.

Sébastien Durand
Cancer Research Centre of Lyon, INSERM U1052, CNRS UMR5682, UCBL
Marion Bruelle
Cancer Research Centre of Lyon, INSERM U1052, CNRS UMR5682, UCBL
Fleur Bourdelais
Cancer Research Centre of Lyon, INSERM U1052, CNRS UMR5682, UCBL, Inovarion
Bigitha Bennychen
University of Ottawa, National Research Council Canada
Juliana Blin
International Center for Infectiology Research https://orcid.org/0000-0002-9628-8920
Caroline Isaac
Cancer Research Centre of Lyon, INSERM U1052, CNRS UMR5682, UCBL
Aurélia Huyghe
Claude Bernard University Lyon 1
Antoine Seyve
Cancer Research Centre of Lyon, INSERM U1052, CNRS UMR5682, UCBL
Christophe Vanbelle
Centre de Recherche en Cancérologie de Lyon
David Meyronet
Cancer Research Centre of Lyon, INSERM U1052, CNRS UMR5682, UCBL
Frederic CATEZ
INSERM U1052, CNRS UMR5286 https://orcid.org/0000-0001-8255-9091
Jean-Jacques Diaz
Cancer Center of Lyon
Fabrice Lavial
Claude Bernard University Lyon 1 https://orcid.org/0000-0001-9752-4393
Emiliano Ricci
Inserm https://orcid.org/0000-0002-9789-5837
François Ducray
Hôpital neurologique
Mathieu Gabut (mathieu.gabut@inserm.fr)

Cancer Research Centre of Lyon, INSERM U1052, CNRS UMR5682, UCBL

Article

Keywords:

Posted Date: February 4th, 2022

DOI: https://doi.org/10.21203/rs.3.rs-738081/v1

RSL24D1 sustains steady-state ribosome biogenesis and pluripotency translational programs in embryonic stem cells.

Authors

Sébastien Durand[1,2*], Marion Bruelle[1,2*], Fleur Bourdelais[1,2,3*], Bigitha Bennychen[4], Juliana Blin-Gonthier[5], Caroline Isaac[1,2], Aurélia Huyghe[2,6], Antoine Seyve[1,2], Christophe Vanbelle[2], David Meyronet[1,2,7], Frédéric Catez[2,8], Jean-Jacques Diaz[2,8], Fabrice Lavial[2,6], Emiliano P. Ricci[5], François Ducray[1,2], Mathieu Gabut[1,2,+].

Affiliations

1. Stemness in gliomas laboratory, Cancer Initiation and Tumoral Cell Identity (CITI) Department.
2. Cancer Research Centre of Lyon (CRCL) INSERM 1052, CNRS 5286, Université Claude Bernard Lyon I, Centre Léon Bérard, Lyon, France.
3. Inovarion, 75005 Paris, France.
4. University of Ottawa, Dept. of Biochemistry, Microbiology and Immunology, Human Health Therapeutics Research Centre, Ottawa, Canada.
5. Laboratoire de Biologie et de Modélisation de la Cellule, ENS de Lyon, CNRS UMR 5239, Inserm U1293, Lyon, France.
6. Cellular reprogramming, stem cells and oncogenesis. Equipe labellisée la Ligue contre le cancer, Labex Dev2Can, CITI Department.
7. Institut de Pathologie Est, Hospices Civils de Lyon, Lyon, France.
8. Ribosomes, translation and cancer laboratory, CITI Department.

* Authors contributed equally to this work.

+ Author for correspondence (mathieu.gabut@inserm.fr)

Abstract

Embryonic stem cell (ESC) fate decisions are regulated by a complex molecular circuitry that requires tight and coordinated gene expression regulations at multiple levels from chromatin organization to mRNA processing. Recently, ribosome biogenesis and translation have emerged as key pathways that efficiently control stem cell homeostasis. However, the molecular mechanisms underlying the regulation of these pathways remain largely unknown to date. Here, we analyzed the expression, in mouse ESCs, of over 300 genes involved in ribosome biogenesis and we identified RSL24D1 as the most differentially expressed between self-renewing and differentiated ESCs. RSL24D1 is highly expressed in multiple mouse pluripotent stem cell models and its expression profile is conserved in human ESCs. RSL24D1 is associated with nuclear pre-ribosomes and is required for the maturation and the synthesis of 60S subunits in mouse ESCs. Interestingly, RSL24D1 depletion significantly impairs global translation, particularly of key pluripotency factors, including POU5F1 and NANOG, as well as components of the polycomb repressive complex 2 (PRC2). Consistently, RSL24D1 is required for mouse ESC self-renewal and proliferation. Taken together, we show that RSL24D1-dependant ribosome biogenesis is required to both sustain the expression of pluripotent transcriptional programs and silence developmental programs, which concertedly dictate ESC homeostasis.

Introduction

Pluripotent stem cells (PSCs), including embryonic stem cells (ESCs) and induced pluripotent stem cells (iPSCs), have the unique abilities to self-renew in a naive state while remaining competent to differentiate into all lineages that compose developing embryos. This ambivalent state is tightly coordinated at different steps of gene

expression, which have been extensively described at the chromatin, transcriptional and post-transcriptional levels [1-4]. This led to the identification of key regulatory epigenetic and transcriptional programs that rapidly rewire gene expression and regulate cell fate transitions in response to environmental cues [2,5,6]. For instance, chromatin modifications mediated by the Polycomb Repressive Complexes 1 and 2 (PRC1 and PRC2) play pivotal roles in the transcriptional regulation of pluripotency and differentiation of PSCs [2,5-7]. However, multiple studies suggest that messenger RNA (mRNA) and protein levels are poorly correlated, including in PSCs, thus highlighting the importance of translational regulations for shaping the cellular proteome landscape required for cell fate changes [8-12]. In addition, recent studies highlighted a lower translation efficiency in undifferentiated ESCs, but also in adult stem cells, compared to differentiated progenies [13]. Taken together, this compelling evidence therefore demonstrates that the regulation of protein synthesis plays a key role in defining stem cell fate.

In eukaryotes, ribosome biogenesis is a complex and multistep process that consecutively involves the nucleoli, the nucleoplasm and the cytoplasm, as well as over 280 ribosome biogenesis factors (RBFs) and different families of non-coding RNAs [14,15]. Many studies have established that ribosome biogenesis is finely regulated in stem cells and may directly control stem cell properties [13]. First, despite a low protein synthesis activity, ESCs display higher levels of rRNA transcription rates compared to endoderm-committed cells [16], and rRNA transcription is finely coordinated with proliferation rates and protein synthesis in mouse ESCs [17,18]. Similarly, several key RBFs are expressed at higher levels in ESCs compared to differentiated progenies, and promote for ESC self-renewal [19-21]. In addition to these essential RBFs, ribosome subunit-specific RBFs are also required to support ESC maintenance. Indeed, several factors implicated in the

maturation of the 40S small ribosome subunit (SSU) are preferentially expressed in naive ESCs compared to differentiated progenies and support the translation of key pluripotency transcription factors (PTFs) such as NANOG [22]. Notably, Notchless, a RBF of the 60S large ribosome subunit (LSU), is required for the Inner Cell Mass survival during early mouse embryogenesis. However in contrast to Notchless functions in adult stem cells homeostasis, it is unclear whether its role in ribosome biogenesis is implicated in this developmental context [23-25]. Therefore, to date, the contributions of ribosome subunit-specific RBFs, especially of the pre-60S, to the steady-state stoichiometry of the 40S and 60S subunits and their impact on the regulation of PSC fate decision remain elusive and should be further investigated.

Here, we show that RSL24D1, a conserved homolog of the yeast pre-60S maturation and export factor Rlp24, is expressed at high levels in mouse and human PSCs compared to differentiated progenies, and is essential for the maturation of the LSU in pluripotent mouse ESCs. RSL24D1 is also required to maintain a steady-state level of translation, in particular of key PTFs such as NANOG and POU5F1, but also of PRC2 factors that maintain repressive H3K27me3 marks over developmental genes to prevent their premature activation. Moreover, high levels of RSL24D1 are required to support mouse ESC proliferation and self-renewal. Altogether, these results establish for the first time that a *bona fide* 60S biogenesis and the resulting translation activity are coordinated with transcription and chromatin regulation networks to control ESC homeostasis.

Results

Rsl24d1 expression is enriched in murine and human PSCs.

To identify factors contributing to ribosome assembly in PSCs, we first defined the mRNA expression profiles of 303 genes, including RBFs and ribosomal proteins (RPs), in

murine PSCs and differentiated cell lines using publicly available RNA-seq data [26] (Supplemental Fig. S1A and Table S1). Although the majority (70%) of these factors were expressed at higher RNA levels (fold change > 1.5) in pluripotent cells compared to differentiated cells (Fig. 1A), Rsl24d1, a predicted ribosome biogenesis protein, displayed the most striking enrichment in PSCs (fold change > 10^4) (Fig. 1A). We next confirmed that, similarly to POU5F1, RSL24D1 was also expressed at a higher level in mouse pluripotent CGR8 ESCs cultured either in serum+LIF (ESC^{FBS}) or in 2i-induced naïve ground state (ESC^{2i}) conditions compared to *in vitro* ESC-derived 12-day old differentiated embryoid bodies (EB^{12}) (Fig. 1B). In contrast, the expression of eL8 (RPL8), a canonical RP of the LSU, remained globally unchanged at the protein level as ESCs differentiate into EBs (Fig. 1B).

We next assessed the dynamics of expression of Rsl24d1 during the kinetics of ESC differentiation, which is correlated to a rapid downregulation of several key PTFs: Pou5f1, Klf4, Nanog and Sox2 (Supplemental Fig. S1B). Interestingly, Rsl24d1 mRNAs and proteins were consistently expressed at higher levels in the ESC^{FBS} condition and progressively decreased after differentiation initiation to reach the lowest expression in EB^{12} (Supplemental Fig. S1B-C). The expression of additional RPs also decreased, yet to a lower extent than RSL24D1, while the downregulation of the biogenesis factors EIF6 and NOG1 rather followed RSL24D1's profile. In addition to CGR8, we assessed the expression of RSL24D1 in two additional mouse ESCs lines (R1 and G4) cultured in similar conditions (ESC^{2i}, ESC^{FBS}, EB^{12}) (Fig. 1C). Although RSL24D1 was expressed at different basal levels in the three ESC models, these results confirmed that RSL24D1 levels were significantly higher in ESCs maintained in pluripotent states than in ESC-derived differentiated EBs. Altogether, these results convincingly demonstrate that RSL24D1 expression is high in murine ESCs and strongly decreases upon differentiation.

We then hypothesized that the expression of Rsl24d1 would rather be determined by the pluripotency status than by the embryonic origin. To evaluate this hypothesis, iPSCs were obtained after ectopic expression of Pou5f1, Klf4, c-Myc and Sox2 in mouse embryonic fibroblasts (MEFs) [27] and the kinetics of somatic reprogramming was confirmed by the activation of endogenous Pou5f1 and Nanog mRNAs (Supplemental Fig. S1D). While eL8 expression remained globally unchanged, RSL24D1 expression was highly increased in 14-day old iPSCs compared to parental MEFs (Fig. 1D). Since the early steps of iPSC formation are stochastic [28], we next investigated Rsl24d1 expression in cells with enhanced reprogramming potential at the single cell level from published data [29]. Interestingly, compared to cells engaged in early steps of the reprogramming path (eRP), Rsl24d1 expression was strongly enhanced in a continuum of cells representing different stages of active reprogramming (pre-PCs) and its levels were even further increased in chimera-competent reprogrammed cells (PCs) expressing high levels of PTFs (Supplemental Fig. S1E). Altogether, these observations suggest that Rsl24d1 expression is significantly enriched in mouse PSCs regardless of their embryonic origins.

We next investigated whether Rsl24d1 expression pattern was evolutionarily conserved in human PSCs. RNA-seq data first indicated that, similarly to their murine counterparts, human PSCs expressed higher levels of *RSL24D1* mRNAs compared to differentiated cell lines or tissues (Fig. 1E) [26]. Western blot analyses of human OSCAR ESCs cultured in self-renewal media (FGF2) and of ESC-derived EBs (Diff.) confirmed a marked decrease of RSL24D1 expression upon differentiation (Fig. 1F) and in adult human tissues (Supplemental Fig. S1F) [30]. In addition, RSL24D1 was expressed at similar levels in both human OSCAR and H9 ESCs maintained either in primed (TL and FGF2) or naive-like (TL2i) conditions [30] (Supplemental Fig. S1G). Taken together, these results indicate that

Rsl24d1 expression pattern is associated to pluripotency and evolutionarily conserved in PSCs.

RSL24D1 is a biogenesis factor associated with nuclear pre-ribosomes in mouse ESCs

The role of RSL24D1 in higher eukaryotes remains unknown, therefore, to gain insight into its molecular functions in mouse ESCs, we first compared its sequence and structure with conserved homologs. Indeed, Rlp24, the yeast homolog of RSL24D1, is a ribosome biogenesis factor involved in the export of nuclear pre-60S ribosomal particles to the cytoplasm where they undergo final steps of maturation, including Rlp24 substitution by the canonical RP eL24 (Rpl24) [15,31]. Multiple protein alignments of yeast Rlp24 to higher eukaryote homologs revealed that the first 130 amino acids of Rlp24 were well conserved from yeast to human (Supplemental Fig. S2A, B). In particular, RSL24D1 homologs were strongly conserved in mammals, with a sequence identity over 96%, but lacked the yeast-specific C-terminal extension of Rlp24.

We next compared the predicted structure of the mouse RSL24D1 with cryo-EM structures of yeast and human protein homologs, which have been recently obtained from nuclear pre-60S intermediates, while they are absent in cytoplasmic pre-60S particles [32,33]. Interestingly, the first 135 amino acids of mouse RSL24D1 almost perfectly matched the yeast Rlp24 and human RSL24D1 structures from pre-60S intermediates (Fig. 2A). Altogether, these results strongly support a conserved function of RSL24D1 in the nuclear maturation of the pre-60S particles in mouse ESCs.

To test this hypothesis, we next analyzed the localization of RSL24D1 in CGR8 ESCs. Since no difference in RSL24D1 expression was observed between the ESC^{2i} and ESC^{FBS} conditions, all following experiments were performed in CGR8 ESC^{FBS}. RSL24D1 was expressed in all colony-forming ESCs regardless of POU5F1 steady-state levels

(Supplemental Fig. S2C) and was predominantly concentrated within nuclear foci containing the RBF Fibrillarin (FBL) (Fig. 2B), therefore suggesting that RSL24D1 is mostly located in ESC nucleoli [34].

We then asked whether RSL24D1 was associated with pre-ribosomal particles in CGR8 ESC^{FBS} colonies. Following cell fractionation, pre-ribosomal and ribosomal particles were respectively isolated from nuclear and cytoplasmic fractions by ultracentrifugation on sucrose cushions. In contrast to eL8 (LSU) and eS6 (RPS6) (SSU) that were both present in nuclear and cytoplasmic ribosomal particles, eL24 (RPL24) was exclusively present in cytoplasmic ribosomes (Fig. 2C). In addition, the LSU biogenesis factor EIF6, homolog of yeast Tif6, co-purified with both nuclear and cytoplasmic ribosomal particles, whereas RSL24D1 was predominantly detected in nuclear pre-ribosomes and slightly associated with cytoplasmic ribosomes (Fig. 2C). Cell fractionation assays confirmed that RSL24D1 was predominantly detected in the nuclear fraction (68%) and to a lower extent in the cytoplasmic fraction (32%), while eL24 was almost exclusively present in the cytoplasm (95%) (Supplemental Fig. S2D). These observations suggest that RSL24D1 is rapidly removed from cytoplasmic pre-ribosomes and most likely replaced by eL24 after nuclear export, in agreement with observations in yeast and human [15,31,32]. To confirm that RSL24D1 is associated with pre-60S particles, cytoplasmic fractions were analyzed by polysome profiling assays to separate the 40S, 60S, 80S (monosomes) and polysomes (Supplemental Fig. S2E). As expected, eL8 and eS6 were predominantly detected in 60S and 40S ribosomal fractions, respectively, and both proteins were also present in monosomes and polysomes (Fig. 2D). In contrast, RSL24D1 and EIF6 were mainly detected in 60S fractions (lane 4), and to a lower extent in 80S fractions (lanes 5 and 6), most likely reflecting an incomplete separation of 80S and 60S, while they were not significantly detected in the 40S fractions (lane 3).

Altogether, these results suggest for the first time that RSL24D1 is a LSU RBF in higher eukaryotes, which is incorporated into nucleolar pre-60S particles, transits to the cytoplasm and is subsequently removed from cytoplasmic pre-60S.

RSL24D1 depletion impairs both ribosome biogenesis and translation

To confirm that RSL24D1 is involved in ribosome biogenesis, we then determined whether its depletion impacts the accumulation and activity of mature cytoplasmic ribosomes. Rsl24d1 siRNA treatment for 72 hours resulted in an efficient depletion of RSL24D1 (> 67%) in CGR8 ESCs compared to control non-targeting siRNAs (Fig. 3A and Supplemental Fig. 3A). Interestingly, RSL24D1 depletion did not detectably affect the structure and the number of FBL-containing nucleoli (data not shown), thus suggesting that decreasing RSL24D1 levels does not significantly impair early ribosome biogenesis.

Next, the effect of RSL24D1 depletion on ribosome production was assessed by polysome profiling assays conducted on control- or Rsl24d1-siRNA treated ESCs. The transient depletion of RSL24D1 caused a significant loss of 60S and 80S relative to 40S subunits (Fig. 3B, C). To achieve a more efficient and stable depletion of RSL24D1, we designed two independent shRNAs targeting Rsl24d1 mRNAs (sh-Rsl24d1-1 and sh-Rsl24d1-2), which resulted in a 51% and 93% depletion of RSL24D1, respectively, compared to control shRNAs (Supplemental Fig. S3B). Interestingly, expressing sh-Rsl24d1-2, which provided the most robust silencing of RSL24D1, also caused an impaired accumulation of the 80S and 60S subunits, to a similar extent than siRNA-treated cells (Supplemental Fig. S3C and S3D).

In order to further characterize the molecular alterations resulting from RSL24D1 depletion, nuclear and cytoplasmic ribosomal fractions were isolated from si-CTL and siRsl24d1-treated ESCs (Fig. 3D). The depletion of RSL24D1 resulted in a significant loss

of EIF6 association with nuclear pre-ribosomes (lanes 3-4) and cytoplasmic particles (lanes 7-8). eL24 inclusion into cytoplasmic ribosomal particles was also strongly impaired upon RSL24D1 knockdown (lanes 7-8), while the presence of the canonical eL8 in both nuclear pre-ribosomes and cytoplasmic ribosomes was not significantly affected (lanes 1-8). Moreover, the consistent decrease of eL24 and EIF6 expression in cytoplasmic (lanes 5-6) and nuclear (lanes 1-2) fractions upon RSL24D1 depletion was further confirmed in total extracts (Fig. 3E). These observations suggest that defects in EIF6 and eL24 association with pre-60S particles might interfere with the stability or translation of these proteins. Altogether, these results indicate that RSL24D1 is required for the *bona fide* maturation of pre-60S particles, at least by allowing EIF6 and eL24 association with nuclear pre-ribosomes and mature cytoplasmic ribosomes, respectively. Hence, RSL24D1 plays a critical role in the production of mature LSU in mouse ESCs.

Finally, we hypothesized that RSL24D1 depletion may also affect global protein synthesis in ESCs. ^{35}S pulse-chase labelling assays were performed on CGR8 ESCs transfected with si-CTL or si-Rsl24d1, in the presence or absence of cycloheximide (CHX), an inhibitor of translation elongation (Fig. 3F). As expected, CHX almost completely abrogated ^{35}S incorporation in newly synthetized proteins (lanes 3-4), while RSL24D1 depletion caused a significant reduction (43%) of *de novo* protein synthesis activity in ESCs (lanes 5-6). Altogether, these results convincingly demonstrate that RSL24D1 is as an essential LSU RBF required for the steady-state protein synthesis in ESCs.

Rsl24d1 is required to maintain pluripotent transcriptional programs

The effects of Rsl24d1 knockdown on ribosome biogenesis and translation are likely to impair the regulation of specific gene programs in mouse ESCs. To address this question, RNA-Seq profiling was performed on CGR8 ESCs transfected with control- or Rsl24d1-targeting siRNAs. The top 15% of genes with the most significant expression changes (>1.8 fold change; $p < 0.01$) were further analyzed. Rsl24d1 loss resulted in the altered expression of 529 genes, including 250 upregulated (47%) and 279 downregulated (53%) genes (Table S2). A Gene Ontology analysis of genes decreased upon Rsl24d1 depletion revealed a significant enrichment in terms associated with immune response and metabolic processes ($p < 0.01$) (Fig. 4A; Supplemental Fig. 4A; Tables S3A and S3B). Conversely, genes upregulated upon si-Rsl24d1 treatment were strongly associated with developmental processes, cell differentiation, proliferation and transcription regulation ($p < 1E-06$) (Fig. 4A; Supplemental Fig. S4A; Tables S3C and S3D). These results suggest that Rsl24d1 expression in mouse ESCs is required to maintain a coordinated regulation of specific transcription programs that control ESC homeostasis and pluripotency.

We next hypothesized that the alterations of ESC transcription programs caused by Rsl24d1 depletion could result from impaired expression of key transcriptional or epigenetic stemness regulators [35]. Indeed, an analysis using the StemChecker algorithm [36] revealed that genes downregulated (n=279) upon Rsl24d1 knockdown were enriched in targets of key PTFs, including Nanog, Pou5f1, Smad4 and Sox2 (Fig. 4B; Table S4A). Conversely, upregulated genes (n=250) were preferentially enriched in targets of essential epigenetic regulators of the polycomb family, including Suz12, Eed and Ezh2 from PRC2, and Rnf2 from PRC1 (Fig. 4B; Table S4B). To establish whether genes differentially expressed upon Rsl24d1 knockdown are direct targets of these PTFs and PRC factors, we next examined the promoter regions of these 529 genes for enrichment in binding sites for these factors, using ChIP-seq assays performed in mouse ESCs (ChIP-

Atlas database [37]) (Fig. 4C, Table S5). Interestingly, promoters of downregulated genes showed a significant 2-fold enrichment in POU5F1 and NANOG binding sites compared to those of upregulated genes. In addition, the promoter regions of upregulated genes were significantly enriched in binding sites for PRC1 and PRC2 factors compared to those of downregulated genes (Fig. 4C). Strikingly, about half of promoter regions of upregulated genes were bound by EZH2 (48,9%), SUZ12 (56,4%), EED (36%) or RNF2 (58,4%) in mouse ESCs (Table S5). These results further confirmed that genes down- or upregulated upon RSL24D1 depletion are enriched in direct targets of POU5F1/NANOG or EZH2/SUZ12/EED/RNF2, respectively.

PRC2 is a key epigenetic repressor responsible for H3K27me2 and H3K27me3 modifications, which control the expression of early commitment genes in ESCs [2,5-7]. Since a large proportion of differentially expressed genes upon Rsl24d1 depletion were associated with PRC2 binding sites, we next analyzed the H3K27 methylation status of their promoter regions using published dataset obtained from mouse ESCs [7] (Supplemental Fig. S4B). While the promoters of down- and upregulated genes were not differentially associated to H3K27me2 marks, they were less associated to H3K27me1 modifications (active transcription) and were rather significantly enriched in H3K27me3 repressive marks. These results suggest that the levels of H3K27me3 may be altered when RSL24D1 is depleted. Accordingly, si-Rsl24d1 treated CGR8 cells displayed lower levels of nuclear H3K27me3 compared to si-CTL treated cells (Supplemental Fig. S4C), suggesting that some of the alterations in gene expression caused by RSL24D1 loss may directly result from this global reduction of H3K27me3.

Finally, we compared RNA-seq predictions from si-Rsl24d1 ESCs with expression profiling from EED and EZH2 knockout mouse ESCs [5,6]. Interestingly, genes displaying an altered expression upon RSL24D1 depletion were enriched in genes that are mis-

regulated in EED$^{-/-}$ or EZH2$^{-/-}$ ESCs (Supplemental Fig. 4D). Strikingly, genes similarly impaired in PRC2 mutant cells and RSL24D1-depleted cells were predominantly upregulated genes (Fig. 4D). Altogether these results suggest that genes up- or downregulated upon RSL24D1 knockdown are likely controlled by distinct molecular mechanisms. On the one hand, downregulated genes are enriched in key PTF targets, suggesting that the transcriptional regulatory activities of POU5F1 and NANOG are decreased in si-Rsl24d1 treated ESCs. On the other hand, the enrichment of H3K27me3 sites and binding sites for PRC2 proteins in promoter regions of upregulated genes suggests that RSL24D1 depletion most likely hinders the repressive activity of PRC2 therefore leading to reduced H3K27me3 deposition and aberrant premature activation of early developmental genes.

The translational regulation of key stemness factors is impaired in RSL24D1-depleted ESCs.

In order to investigate how RSL24D1 modulates the activity of PTFs and PRC2 factors, we first measured whether RSL24D1 loss affected their transcription. Interestingly, the mRNA levels of these PTFs and PRC factors were not strongly impaired in si-Rsl24d1 ESCs, except for Nanog (Supplemental Fig. S5A), suggesting that rather the production or the activity of the corresponding proteins might be affected by RSL24D1 depletion.

Since RSL24D1 loss decreases global protein synthesis, the alteration of PRC2 activity could result from a perturbation of Eed, Ezh2 and Suz12 mRNA translation. Thus, we analyzed the association of these mRNAs with the different ribosomal fractions in CGR8 cells treated with either si-CTL or si-Rsl24d1 (Supplemental Fig. S5B and S5C) by RT-qPCR. As expected, the majority (>92%) of Eed, Ezh2 and Suz12 mRNAs were associated with polysomes and therefore actively translated in self-renewing ESCs (Fig. 5A and Supplemental Fig. S5C, gray curves). However, RSL24D1 depletion significantly reduced

the association of Eed and Ezh2 mRNAs with polysomal fractions while increasing their detection in free mRNPs and monosomes (Fig. 5A and Supplemental Fig. S5C, black bars). While the switch of Suz12 mRNAs from polysomal to monosomal fractions upon depletions was not statistically significant, likely due to biological variability in the extend of depletion effects (Fig. 5A), analyses of the polysome fractions alone seemed to indicate that Suz12 mRNAs also tend to transit from heavy to light polysomes upon RSL24D1 depletion (Supplemental Fig. S5C).

To further confirm that RSL24D1 downregulation impaired the translation of Suz12, Eed and Ezh2 mRNAs, steady-state expression levels of corresponding proteins were assessed by semi-quantitative western blots on CGR8 total extracts. Interestingly, RSL24D1 depletion induced a significant reduction of EED and SUZ12 levels, albeit no significant downregulation was observed for EZH2 (Fig. 5B). Altogether, these observations suggest that the loss of PRC2 activity upon RSL24D1 depletion is likely caused by a defect in the translation of Eed, Ezh2 and Suz12 mRNAs in ESCs.

Similar to PRC2 factors, we hypothesized that a decrease in POU5F1 and NANOG mRNA translation may be responsible for the downregulation of specific genetic programs enriched in POU5F1 and NANOG target genes. Accordingly, semi-quantitative western blots demonstrated a significant reduction in both POU5F1 and NANOG levels in si-Rsl24d1 treated cells compared to si-CTL cells (Fig. 5C). Immunostaining experiments confirmed that the POU5F1 downregulation in si-Rsl24d1 treated ESCs did not result from the emergence of POU5F1-negative differentiated cells but rather resulted from a global decrease in POU5F1 expression (Supplemental Fig. S5D). Altogether, these results confirm that RSL24D1 depletion directly impairs the translation and the accumulation of both key PTFs and core PRC2 factors, which respectively play pivotal roles in controlling

gene expression programs and the chromatin landscape underlying cell fate decisions in ESCs.

High RSL24D1 expression supports the maintenance of self-renewal capacities but is dispensable for ESC differentiation.

Since transient RSL24D1 depletion altered the expression of several PTFs and promoted the activation of genes involved in developmental programs, we examined the functions of RSL24D1 for ESC fundamental self-renewal and differentiation capacities. First, stable RSL24D1 downregulation by constitutively expressed shRNAs (Supplemental Fig. S3B) significantly impaired, in a dose-dependent manner, the proliferation of CGR8 cells in both real-time assays (Fig. 6A) and long-term kinetics of proliferation (Fig. 6B). We next analyzed whether the mRNA expression of several major PTFs was affected by stable long-term depletion of RSL24D1 in CGR8 cells. In contrast to si-Rsl24d1 transient knockdowns, RT-qPCR assays revealed a significant downregulation of Nanog, Pou5f1 and Sox2 in cells expressing Rsl24d1 shRNAs, while Klf4 expression remained globally unaffected (Supplemental Fig. S6A). Western blot assays confirmed a significant downregulation of POU5F1 in sh-Rsl24d1-2 expressing CGR8 ESCs (Supplemental Fig. S6B). Thus, these observations suggest that RSL24D1 stable depletion likely affected self-renewal capacities. To confirm this hypothesis, CGR8 ESCs expressing non-targeting shRNAs (sh-Control), or shRNAs targeting Pou5f1 or Rsl24d1 mRNAs were seeded at clonal density to recapitulate the formation of individual undifferentiated colonies displaying high levels of alkaline phosphate (AP) activity [38]. As expected, POU5F1 downregulation led to a drastic reduction (>90 %) in the number of AP positive colonies compared to control shRNA treated cells (Fig. 6C and Supplemental Fig. S6C). Similarly, RSL24D1 depletion caused a dose-dependent and significant reduction (>50%) of AP-

positive ESC colonies (Fig. 6C and Supplemental Fig. S6C), suggesting that a high expression of RSL24D1 in mouse ESCs is required to support both self-renewal and proliferation.

Finally, we compared the differentiation capacities of sh-Control, sh-Pou5f1 and sh-Rsl24d1-1/2 expressing CGR8 cells by EB differentiation assays. As expected, POU5F1 knockdown strongly impaired the capacities of CGR8 cells to form viable 12 day-old EBs, whereas RSL24D1 downregulation had no significant impact on EB formation compared to sh-Control ESCs (Fig. 6D). Moreover, the depletion of POU5F1 almost completely abolished the presence of fully differentiated cardiomyocytes, which are responsible for spontaneous EB beating (Fig. 6E) [39], likely reflecting its role in early cell fate determination [40,41]. Conversely, RSL24D1 stable knockdowns only partially impaired the formation of functional cardiomyocytes from ESCs (Fig. 6E). Thus, RSL24D1 is required for ESC self-renewal and proliferation but is however dispensable, at least partially, for differentiation.

Discussion

Despite displaying reduced translation activity compared to differentiated progenies [13], ESCs paradoxically express RBFs and RPs at higher levels than differentiated cells [20-22]. This observation therefore suggests that naive ESCs may need to accumulate, at a steady-state level, a pool of ribosomes sufficient to sustain rapid proteome changes and increased translational activities required to achieve all possible programs of differentiation in response to environmental signals. In order to better define molecular mechanisms and factors coordinating the highly regulated production of ribosomes in ESCs, we characterized RSL24D1, a homolog of the yeast LSU ribosome biogenesis factor Rlp24, which is consistently expressed at high levels in PSCs, including mouse ESCs and

iPSCs, and rapidly downregulated after differentiation induction. We determined that RSL24D1 is predominantly localized in nucleoli of mouse ESCs, which are nuclear domains playing a central role in the early steps of pre-ribosome assembly, and, to a lower extent, in the cytoplasm. In contrast, FBL and eL24 were almost exclusively detected in the nucleoli and cytoplasm, respectively, as described in yeast. Considering the strong conservation of RSL24D1 structure and localization relative to its yeast homolog Rlp24, it is therefore likely that RSL24D1 shuttles between the nucleus and the cytoplasm [31]. In yeast, Rlp24 is assembled at the initial steps of pre-60S maturation [42], together with Tif6, Nog1 and Mak11 [15,43], and then allows the recruitment of the hexameric Drg1 AAA-ATPase [31,44]. As the pre-LSU particles exit the nucleus, Drg1 gets activated by nucleoporins and releases Rlp24 by mechanical force, therefore allowing its substitution by the canonical ribosomal protein eL24 [31,44,45]. Although Rlp24 deletion in yeast induced moderate alterations of the 35S and 27SB rRNA intermediates, we did not observe any significant modifications of the rRNA processing in si-Rsl24d1 ESCs (data not shown). Consistently, both conditional Rlp24 mutants in yeast [31] and the depletion of RSL24D1 in human cells [46] did not strongly impact the accumulation of intermediate or mature LSU rRNAs. The depletion of RSL24D1 in mouse ESCs rather causes a loss of EIF6 association to nuclear pre-ribosomes and an impaired association of eL24 with cytoplasmic ribosomes (Fig. 3D). Interestingly, RSL24D1 and EIF6, the homolog of yeast Tif6, show different dynamics of disassembly from cytoplasmic ribosomes (Fig. 2C) with EIF6 dissociation occurring belatedly as it is more stably associated with cytoplasmic ribosomal particles. These observations are therefore consistent with the yeast model describing Tif6 removal as the latest maturation step of 60S particles [15,47]. In addition to these molecular alterations, RSL24D1 depletion in mouse ESCs caused a decrease of 60S and 80S subunits relative to 40S particles, consistently with observations upon Rlp24

depletion in yeast [31] or 60S biogenesis repression [25,48]. Moreover, we detected the presence of half-mers for di- and tri-ribosomes in si-Rsl24d1 treated cells (Fig. 3B), which were previously observed upon LSU biogenesis alterations in yeast [49,50]. Altogether, our data strongly support evolutionary conserved functions for RSL24D1 to guide RBF association in early steps of LSU assembly, as well as to stabilize ribosome structure locally by protein mimicry until late cytoplasmic maturation steps where it is replaced by eL24.

At the physiological level, we showed that RSL24D1 depletion caused a significant loss of proliferation and self-renewal capacity while having a moderate impact on ESC differentiation *in vitro*. This is in agreement with RSL24D1 expression profile, which is high in pluripotent ESCs but low in differentiating progenies. Surprisingly, attempts to overexpress an exogenous FLAG-RSL24D1 protein, at near endogenous levels, induced a rapid and stable downregulation of endogenous RSL24D1 in ESCs (data not shown). This therefore suggests that PSCs finely tune the steady-state level of RSL24D1, most likely to avoid aberrant RSL24D1 levels that could be detrimental for ribosome biogenesis and stem cell homeostasis. We propose a model where RSL24D1 actively contributes to the biogenesis of pre-60S particles and to the accumulation of mature monosomes and polysomes in the cytoplasm of naive mouse ESCs (Fig. 7). We also suggest that RSL24D1 is highly expressed and shuttles back and forth between the nucleoli and the cytoplasm to support an elevated rate of 60S biogenesis in ESCs while its activity is less required in differentiating ESC progenies.

We then established that the impaired accumulation of LSUs in the cytoplasm caused by RSL24D1 depletions strongly reduced global protein synthesis similarly to downregulations of either HTATSF1, which controls rRNA processing, or SSU biogenesis factors in mouse ESCs [18,22]. In addition to a global translational impact, we provided

evidence that RSL24D1 depletions reduce levels of specific instable proteins including POU5F1 and NANOG. Notably, NANOG decrease may result from combined transcriptional and translation defects while POU5F1 downregulation was not detected at the transcriptional level in the same conditions (Fig. 5C and Supplemental Fig. 5A). A highlight of this study is that the steady-state level of several PRC2 factors, including EZH2, EED and SUZ12 is tightly controlled by the level of ribosome biogenesis in ESCs. Although these factors play a key role in organizing the landscape of transcriptionally silent chromatin by maintaining H3K27me3 modifications, particularly on promoters of repressed developmental genes, their activity rather seems rate-limiting as slight changes in expression have a large impact on gene regulation in ESCs. Indeed, the downregulation of RSL24D1 in mouse ESCs induced a reduction in Eed, Suz12 and Ezh2 mRNAs association to polysomes, which most likely affects the neo-synthesis of corresponding proteins. Accordingly, we observed a reduction ranging from 7% to 35% in EED, SUZ12 and EZH2 protein levels. Despite a modest PRC2 protein level decrease, we observed a significant increased expression, at the transcriptional levels, of hundreds of PRC2 target genes normally associated to repressive H3K27me3 marks. Many of these PRC2 target genes correspond to developmental genes, including members of the HOX (HOXB1, 2, 3, 9 and C13) and WNT families (WNT2B, 3, 10A and 10B), transcription factors such as NKX1-2, NKX2-9, POU4F3, SALL3 and NEUROD1. Altogether, this therefore suggests that the versatile status of ESCs, which must rapidly switch from a transcriptionally active self-renewal program to the activation of poised differentiation programs, requires a finely tuned translation of PRC2 factors that is coordinated with ribosome biogenesis in ESCs.

Interestingly, RSL24D1-mediated ribosome biogenesis therefore appears to have a dual role in maintaining ESC self-renewal and proliferation (Fig. 7). On the one hand,

RSL24D1 maintains a balanced expression of key PTFs, including POU5F1 and NANOG, to control pluripotency transcriptional programs. Furthermore, RSL24D1 is a predicted target gene of POU5F1 and NANOG (Table S4 and ChIP-Atlas database), and POU5F1 depletion by shRNAs is correlated to a significant reduction in RSL24D1 protein (>60%, data not shown) in CGR8 cells, suggesting that RSL24D1 expression could be directly controlled by POU5F1 or NANOG in mouse ESCs. On the other hand, RSL24D1 sustains steady-state translation of PRC2 factors and therefore maintains repressive H3K27me3 chromatin marks to prevent the premature activation of developmental genes in naive ESCs (Fig. 7). Intriguingly, EZH2 was recently shown to enhance 2'-O-methylation of rRNAs by promoting the interaction between NOP56 and FBL in mouse extraembryonic endoderm stem cells [51]. This observation raises the question of whether RSL24D1 might influence rRNA 2'-O-methylation by modulating EZH2 expression in naive and differentiated ESCs. Altogether, these results therefore further support that RSL24D1 may be at the core of a regulatory loop that engages the regulation of ribosome biogenesis and translation with chromatin epigenetic and transcription regulations in order to precisely control ESC self-renewal and pluripotency properties.

Finally, modulating the production of ribosomes could also be a mechanism to control the translation of specific subsets of mRNAs that regulate ESC fate. Indeed, it is puzzling that despite an active ribosome biogenesis, ESCs display a globally reduced translational activity. One hypothesis could be that mouse ESCs have a short cell cycle that could stimulate ribosome biogenesis. Alternatively, the ribosome concentration may regulate substrate selectivity and maintaining a high ribosome biogenesis, and therefore concentration, could allow the translation of specific programs. This "Ribosome Concentration" model has been previously discussed [52] and may explain why the translation of ESC-relevant mRNAs requires such an elevated amount of ribosomes.

Consistently, upstream open reading frames (uORFs) are commonly used in naive ESCs compared to differentiated cells [53], and mRNAs coding for key PTFs, including Nanog, possess multiple uORFs which specifically enhance their translation in ESCs [54]. Hence, uORF-carrying mRNAs may require a certain amount of ribosomes to be correctly translated in the context of ESCs. One could therefore propose that proper levels of ribosome biogenesis in ESCs is required to control the translation of specific gene programs. Along these lines, ribosome biogenesis defects impacting gene-specific regulations have been proposed to participate to the etiology of congenital disorders called ribosomopathies, which are caused by mutations in RBFs or RPs [52]. Therefore, better defining the molecular feedbacks between ribosome biogenesis, translation and additional key steps of gene expression, including chromatin modifications and transcription, could not only benefit to a developmental research but also to open novel avenues to consider disease treatments.

Methods

Cell culture

Mouse CGR8 ESCs (ECACC General Collection, 07032901) were cultured on 0.2% gelatin-coated plates either in ESC^{FBS} conditions using GMEM BHK-21 (Gibco) supplemented with 10% ESC-grade heat-inactivated Fetal Bovine Serum (HI-FBS), 1x non-essential amino acid (NEAA, Gibco), 2 mM sodium pyruvate (Gibco), 100µM β-mercaptoethanol (BME, Sigma-Aldrich), 10^3U/ml Leukemia Inhibitory Factor (LIF, StemCells Technologies) or in ESC^{2i} conditions using 45% DMEM/F12 (Gibco), 45% Neurobasal medium (Gibco), 100 µM BME, 1.65% Bovine Serum Albumin Fraction V (Gibco), 1X penicillin-streptomycin (P/S, Gibco), 1% N2 supplement (Gibco), 2% B27 supplement (Gibco), 1X ESGRO 2i supplement (Millipore) and 10^3U/ml LIF (Millipore).

Mouse ESC lines R1 and G4 were cultured on irradiated MEFs in ESC^{FBS} media.

Total cell extracts of H9 and OSCAR human ESCs were provided by the Savatier laboratory [30] (Stem cell and Brain Research Institute, Bron, France).

HEK-293T cells were cultured in DMEM (Invitrogen) supplemented with 10% HI-FBS, 1X NEAA, 2 mM sodium pyruvate and 1X P/S. All cell lines were confirmed mycoplasma-free (Lonza, MycoAlert kit).

MEF isolation

MEFs were isolated from $R26^{rtTA}$;$Col1a1^{4F2A}$ E13.5 embryos after removal of the head and internal organs [55]. The remaining tissues were physically dissociated and incubated in trypsin 10 minutes at 37°C. Dissociated cells were resuspended in MEF medium (DMEM supplemented with 10% fetal bovine serum, 100 U/mL penicillin / streptomycin, 1mM sodium pyruvate, 2mM L-glutamine, 0.1mM Non Essential Amino Acids and 0.1mM β-mercaptoethanol).

iPSCs reprogramming

$R26^{rtTA}$;$Col1a1^{4F2A}$ MEFs were plated in six-well plates at 10^5 cells per well in MEF medium for 24h and then in MEF medium containing 2µg/mL doxycyclin [55]. MEFs were reseeded after 72h on 0.1% gelatin-coated plates in iPSC medium (DMEM containing 15% KnockOut Serum Replacement, 10^3 U/mL LIF, 100 U/mL P/S, 1 mM sodium pyruvate, 2 mM L-glutamine, 0.1 mM NEAA and 0.1mM BME). The medium was replaced everyday with doxycyclin-containing fresh medium for 14 days.

Differentiation assays

Embryoid body (EB) formation was performed by the hanging drop method [39]. Briefly 400 cells were cultured in 20 µL hanging drops for 2 days in GMEM BHK-21 supplemented with 20% HI-FBS, 1x NEAA, 2 mM Sodium Pyruvate, 100 µM BME. EBs were then collected in non-adherent culture dishes and cultured for 3 additional days. At Day 5, cell aggregates were cultured on 0.2% gelatin-coated dishes with 10nM retinoic acid (Sigma-Aldrich) and the media was changed every 2 days.

Plasmids

pLKO.1-puro plasmids (Addgene #8453) were cloned as previously described[56]. Briefly, the pLKO.1 plasmid was digested with EcoRI and AgeI restriction enzymes. Linear plasmids were ligated with annealed oligomers containing the shRNA sequence flanked by EcoRI and AgeI restriction sites. All clones were sequenced to confirm the insertion of each shRNA sequence prior to lentiviral production. shRNA sequences used in this study are reported in Table S6A.

Lentiviral production and infection:

Lentiviral particles were produced as previously described [56]. 3 days after cell transfection using FuGENE HD (Promega), each cell media was concentrated using centricon column (Vivaspin 20, Sartorius) and each viral production was titrated. ESCs were infected with an MOI=1 for 16 h in ESC^{FBS} conditions supplemented with 8 µg/mL polybrene (Sigma-Aldrich). 24 h after infection, cells were selected with 1.5 µg/mL of puromycin (Sigma-Aldrich) for at least 48 hours. shRNA sequences are available in Supplemental Table S6A.

siRNA Transfection

ESC^{FBS} CGR8 cells were transfected with 20 nM siRNAs using DharmaFECT 1 (Horizon Discovery) according to the manufacturer's protocol, and collected at 72 h. siRNA sequences are available in Supplemental Table S6A.

Colony-formation assay

ESCs were plated at clonal density (100 cells per cm2) on gelatin-coated plates in ESC^{FBS} conditions. After 7 days, culture dishes were imaged and alkaline phosphatase-positive colonies were detected (Alkaline Phosphatase detection kit, Merck-Millipore) and quantified using ImageJ analysis software [57].

Proliferation assays

The proliferation was first assessed using the x-CELLigence Real-Time Cell Analysis (RTCA) system (ACEA Biosciences, San Diego, CA, USA). 5000 cells were seeded in a 96 E-plates (Roche) and the electrical impedance was acquired every 15 min for 3 days to establish a cell index value extracted from the linear regression of the proliferation curve using the RTCA software.

In addition, the proliferation was also monitored using the high-definition automated imaging system IncuCyte (Essen BioScience), according to the manufacturer's instructions. 750 cells were seeded in 24-well plates. Proliferation rates were estimated from 2 h interval snapshots according to the manufacturer's instructions.

Western Blots

Cells were lysed in 1x Laemli buffer (50mM Tris-HCl pH 6.8, 2% SDS, 5% BME, 10% glycerol and 0.05% bromophenol blue) and protein extracts were analyzed by SDS-polyacrylamide gel electrophoresis (SDS-PAGE) followed by western blotting using

antibodies indicated in Supplemental Table S6B. For total protein quantification, 0.5% trichloroethanol (TCE)(Sigma-Aldrich) was included in the SDS-PAGE prior to electrophoresis and activated post-migration with UV light for 45 sec. Chemiluminescent and fluorescent signals were acquired on ChemiTouch MP imaging system (Bio-rad) and quantified using ImageLab software (Bio-rad). Serial sample dilutions were loaded onto gels to verify the linearity of quantified signals.

Immunofluorescence assays

ESC^{FBS} were cultured on 0.2% gelatin-coated coverslip or 96-well plates. 48 h after siRNA transfections, ESCs were fixed 10 min in 4% formaldehyde and permeabilized 10 min in 0.1% Triton X-100. Cells were incubated 1 h in blocking solution (1X PBS, 0.1% tween 20, 5% BSA) and then with primary and secondary antibodies (Table 6B). Images were acquired using a Zeiss Axio Imager M2 microscope coupled with the Zen 2 Pro software (Zeiss) and processed with ImageJ.

High-Content analysis System (HCS) analyses

For deeper statistical results, cells were plated on a 96 well carrier plate (Perkin Elmer) optimized for sensitive and resolved fluorescence microscopy. At least 90% of the well surface is acquired in one non-confocal plane with Harmony software on an Operetta CLS Flex High-content-Screening system (Perkin Elmer) equipped with 20x/NA1.0 water objective. The set-up was optimized to reach at least a difference of 10000 fluorescence levels between the noise and the signal of interest to allow a robust images analysis and quantification. Data were analyzed with Columbus software (Perkin Elmer). Briefly, on the image of full wells, colonies were located on the nuclei labeling with the appropriate tuned find image region algorithm. To discard small and large colonies,

areas in the range of 500 to 40 000 μm^2 of cells were selected. Then cells in each colony were found with the appropriate tuned find nuclei algorithm. Cell debris and objects with more than one nucleus were excluded by filtering the nuclei according to roundness and surface. Fluorescence intensities are calculated for each selected cellular region for all wells.

Histone Immuno-histochemistry assays

Cells were centrifugated during 10 min at 377g and fixed in an alcohol based fixative solution Thinprep® (Hologic) during 15 min. After centrifugated during 5 min at 377g, the cells were resuspended in 10ml of Epredia™ Gel (Richard-Allan Scientific™ HistoGel™). The gel was hardened during 15 min at 4°C and the corresponding blocks were dehydrated and embedded in paraffin. 3µm-sections were immunostained using an antibody anti-histone H3 containing the trimethylated lysine 27 (H3K27me3) (Diagenode). Heat induced antigen retrieval was done using CC1 basic buffer (Ventana). Staining was performed using DAB Ultraview dection system (Ventana).

Cell fractionation

ESCs were collected and gently lysed for 10 min on ice in hypotonic buffer (HB) containing 10 mM KCl, 0.5 mM $MgCl_2$, 10 mM Tris-HCL pH 7.4, 1X cOmplete EDTA-free protease inhibitors™ (Roche) and 1U/µL RNAseOUT (Invitrogen). 0.02% NP-40 was subsequently added for 5 min and nuclei/cytoplasm were then separated by centrifugation. Nuclei were washed with HB supplemented with 0.01% NP-40 and resuspended in Buffer A (250 mM Saccharose, 250 mM KCl, 5mM $MgCl_2$ and 50 mM Tris-HCl pH7.4) with DNAse I (2000U/mL). Cytoplasmic fractions in HB were adjusted to 250 mM KCL.

Ribosome purification on sucrose cushion

Cytoplasmic and nuclear fractions were loaded on 1 mL sucrose cushion (1M saccharose, 250 mM KCl, 5 mM $MgCl_2$ and 50mM Tris HCl pH7.4) and centrifugated at 250.000 g for 2 h at 4°C. Pellets were washed twice with cold water and resuspended in Buffer C (25 mM KCl, 5 mM $MgCl_2$ and 50 mM Tris-HCl pH 7.4).

Polysome profiling

ESCs were treated with 25 µg/mL of emetine (Sigma-Aldrich) for 15 min and lysed in 10 mM Tris-HCL pH7.5, 5 mM $MgCl_2$, 100 mM KCl, 1% Triton X-100, 2 mM DTT, 1U/µL RNAseOUT and 2X cOmplete EDTA-Free protease inhibitors. Lysates were centrifugated at 1300 g for 10 min to pellet nuclei. Supernatants corresponding to cytoplasmic fractions were then loaded on 10%-50% sucrose gradients poured using the Gradient Master (Serlabo Technologies) and centrifugated at 210.000 g for 2h35 at 4°C. 700 µl fractions were collected using the TELEDYNE ISCO collector while concomitantly acquiring corresponding 254nm absorbance.

RNA extraction

From cells - Cells were harvested in 1ml of TRIzol reagent (Invitrogen) and total RNA was extracted according to manufacturer's instructions. 1 µg of RNA were used for reverse transcription assays using SuperScript II reverse Transcriptase Mix (Invitrogen) according to manufacturer's instructions.

From sucrose gradients - 50 pg of LUCIFERASE RNA (Promega) was added to 250 µl of collected fractions and RNA was extracted with 750 µl of TRIzol LS (Invitrogen)

according to manufacturer's instructions. cDNAs were synthetized using SuperScript™ II Reverse Transcriptase (Invitrogen).

Real Time qPCRs

Quantitative PCR assays were performed using SYBR Green (Roche, Applied Biosystem) following the manufacturer's instructions. Relative cDNA expression was normalized either by β-Actin, Psmd9, Tbp and 603B20Rik mRNA levels (total cell RNA) or Luciferase mRNAs (sucrose gradient RNA). Serial dilutions were systematically performed to calculate qPCR efficiency, verify amplification linearity and determine normalized relative cDNA concentrations. Primers are listed in Supplemental Table S6C.

Metabolic labeling of protein synthesis.

Cells were transfected with siRNAs in 6-well plates 48 h before metabolic labeling. Cells were then incubated for 5 min at 37°C with 55 µCi/well of 35S-L-methionine and ^{35}S-L-cysteine Promix (Perkin Elmer). To validate the labeling efficiency, cycloheximide (100mg/mL final) was added for 10 min prior to labeling. Cells were then washed with 1 ml of ice-cold PBS and lysed in 500µL of RIPA buffer mixed with 1X final LDS Novex™ 4X Bolt™ loading buffer (ThermoFisher). Extracts were then run on precast Bis-Tris Bolt™ 4 to 12% acrylamide gels (ThermoFisher) before staining with the Simply Blue Safestain (Thermo) according to manufacturer's guidelines to visualize total protein loading across lanes. The gel was then incubated in 30% ethanol, 10% acetic acid and 5% glycerol for 1 h and dried at 75°C for 1h30. ^{35}S radioactivity levels were measured using the Typhoon Phosphor imager.

RLP24 homologs protein alignments.

The following protein sequences were considered for protein alignments. For RLP24 homologs: *S. cerevisiae* (Q07915), *C. elegans* RLP24 (Q17606), *D. rerio* RLP24 (Q7ZTZ2), *M. musculus* RSL24D1 (Q99L28), R. *norvegicus* RSL24D1 (Q6P6G7), *B. Taurus* RSL24D1 (Q3SZ12), *H. sapiens* RSL24D1 (Q9UHA3). For RL24 homologs: *S. cerevisiae* RL24A (P04449), *S. cerevisae* RL24B (P24000), *M. musculus* RL24 (Q8BP67). Multiple protein alignments were performed with the Clustal Omega software (https://www.ebi.ac.uk/Tools/msa/clustalo/) [58] and visualized with the Jalview software (http://www.jalview.org/) [59].

RSL24D1 protein structure predictions.

yeast RLP24 and human RSL24D1 structures were obtained from cryo-EM pre-60S structures available in the Protein Data Bank: PDB-6N8J (2019, 3,50Å resolution) [33], PDB-6LSS (2018, 3,70Å resolution) [32]. Mouse RSL24D1 protein structures were modeled based on these 2 cryo-EM protein structures using the SWISS-MODEL structures assessment tool (https://swissmodel.expasy.org/assess) [60-62] and were overlapped using the Pymol software.

RNA-Seq sequencing and analysis.

RNA libraries were prepared with the TruSeq Stranded Total-RNA kit and sequenced using an Illumina NovaSeq 6000. Raw sequencing data quality controls were performed with FastQC (0.11.5) and aligned on the mouse genome (GRCm38) with STAR (2.7.0f). RNA quality control metrics were computed using RSeQC (3.0.0) [63]. Gene expression was quantified using Salmon (0.14.1) from raw sequencing reads, using the annotation of protein coding genes from gencode vM20 as index. The analyses were performed using R (3.6.1). Starting from salmon transcript quantification, we used Tximport (v1.12.3) [64]

and DESeq2 (v1.24) [65] to perform the differential expression analyses (Wald test, and p-value corrections with the Benjamini-Hochberg method). RNA-seq predictions for mouse and human PSCs, differentiated cells and tissues were obtained from a published dataset (GSE45505) [26].

GO enrichment analysis

The analysis of overrepresented gene ontology (GO) categories were conducted using a reference set of 15093 genes expressed in CGR8 cells and using BiNGO (v3.0.3) [66] as well as the open source bioinformatics software platform Cytoscape (v3.7.2) [67] for visualization of the results. Only annotations with p-values < 0.01 (after Benjamini-Hochberg correction) were considered for further analysis.

Target genes analysis with StemChecker

Differentially expressed genes in Rsl24d1-depleted cells were analysed using the web-server StemChecker (http://stemchecker.sysbiolab.eu/) [36], without masking the cell proliferation and cell cycle genes.

Analysis of binding sites defined by ChIP-seq

To identify binding sites for TFs and chromatin-associated factors in the ±1 kb region of TSSs, we combined all datasets available in the ChIP-Atlas database [37] corresponding to mouse wild type ESCs and mouse differentiated cell types for each factor. Binding sites preferentially bound by selected factors in ESCs were selected if they present a ratio of ESC average score / Differentiated average score >2.

Data availability

The publicly available dataset used in this study can be accessed under the GEO accession codes GSE45505, GSE89211, GSE116603 and GSE85717. The RNA-seq data profiles used in this study are under submission at NCBI GEO. All other data supporting the findings of the study are available in this article, its supplementary information files or from the corresponding author upon reasonable request.

Competing Interest Statement

The authors declare no competing interests.

Acknowledgments

We thank Drs. P. Savatier and P.Y. Bourrillot (SBRI, Bron, France) for providing protein extracts of human ESCs, Dr. M. Zeisel for PRC2 antibodies (CRCL, Lyon, France) and Pr. A. Nagy (University of Toronto, Canada) for providing the R1 and G4 cell lines. We thank R. Pommier and A. Viari from the Gilles Thomas Bioinformatics Platform (CRCL, Lyon, France) for the RNAseq analysis. This study was supported by a Marie Curie Career Integration Grant 631794 from the European Union and by an AVENIR grant from the Institut National de la Santé et de la Recherche Médicale (INSERM) to M.G., by a Ph.D. fellowship from La Ligue Nationale Contre le Cancer (M.B.), and by grants from Labellisation de la ligue contre le cancer, Agence Nationale pour la Recherche (ANR) and Institut National du Cancer (INCa) (A.H. and F.L.).

Author contributions: S.D., M.B. and M.G. designed the research. S.D., M.B., F.B., B.B., J.B., C.I., A.H., D.M. performed the research. S.D., M.B., C.V., F.C., J.J.D., F.L, E.R., F.D. and M.G. analyzed the data. S.D., M.B., F.B. and M.G. wrote the manuscript. All authors discussed the results and commented on the manuscript.

References

1 Gabut, M. *et al.* An alternative splicing switch regulates embryonic stem cell pluripotency and reprogramming. *Cell* **147**, 132-146, doi:S0092-8674(11)00949-4 [pii] 10.1016/j.cell.2011.08.023 (2011).

2 Gokbuget, D. & Blelloch, R. Epigenetic control of transcriptional regulation in pluripotency and early differentiation. *Development* **146**, doi:10.1242/dev.164772 (2019).

3 Kolodziejczyk, A. A. *et al.* Single Cell RNA-Sequencing of Pluripotent States Unlocks Modular Transcriptional Variation. *Cell Stem Cell* **17**, 471-485, doi:10.1016/j.stem.2015.09.011 (2015).

4 Vissers, C., Sinha, A., Ming, G. L. & Song, H. The epitranscriptome in stem cell biology and neural development. *Neurobiol Dis* **146**, 105139, doi:10.1016/j.nbd.2020.105139 (2020).

5 Cruz-Molina, S. *et al.* PRC2 Facilitates the Regulatory Topology Required for Poised Enhancer Function during Pluripotent Stem Cell Differentiation. *Cell Stem Cell* **20**, 689-705 e689, doi:10.1016/j.stem.2017.02.004 (2017).

6 Lavarone, E., Barbieri, C. M. & Pasini, D. Dissecting the role of H3K27 acetylation and methylation in PRC2 mediated control of cellular identity. *Nat Commun* **10**, 1679, doi:10.1038/s41467-019-09624-w (2019).

7 Juan, A. H. *et al.* Roles of H3K27me2 and H3K27me3 Examined during Fate Specification of Embryonic Stem Cells. *Cell reports* **17**, 1369-1382, doi:10.1016/j.celrep.2016.09.087 (2016).

8 Kristensen, A. R., Gsponer, J. & Foster, L. J. Protein synthesis rate is the predominant regulator of protein expression during differentiation. *Mol Syst Biol* **9**, 689, doi:10.1038/msb.2013.47 (2013).

9 Lu, R. *et al.* Systems-level dynamic analyses of fate change in murine embryonic stem cells. *Nature* **462**, 358-362, doi:10.1038/nature08575 (2009).

10 Maier, T., Guell, M. & Serrano, L. Correlation of mRNA and protein in complex biological samples. *FEBS Lett* **583**, 3966-3973, doi:10.1016/j.febslet.2009.10.036 (2009).

11 Munoz, J. *et al.* The quantitative proteomes of human-induced pluripotent stem cells and embryonic stem cells. *Mol Syst Biol* **7**, 550, doi:10.1038/msb.2011.84 (2011).

12 Schwanhausser, B. *et al.* Global quantification of mammalian gene expression control. *Nature* **473**, 337-342, doi:10.1038/nature10098 (2011).

13 Gabut, M., Bourdelais, F. & Durand, S. Ribosome and Translational Control in Stem Cells. *Cells* **9**, doi:10.3390/cells9020497 (2020).

14 de la Cruz, J. *et al.* Feedback regulation of ribosome assembly. *Curr Genet* **64**, 393-404, doi:10.1007/s00294-017-0764-x (2018).

15 Klinge, S. & Woolford, J. L., Jr. Ribosome assembly coming into focus. *Nature reviews. Molecular cell biology* **20**, 116-131, doi:10.1038/s41580-018-0078-y (2019).

16 Woolnough, J. L., Atwood, B. L., Liu, Z., Zhao, R. & Giles, K. E. The Regulation of rRNA Gene Transcription during Directed Differentiation of Human Embryonic Stem Cells. *PLoS One* **11**, e0157276, doi:10.1371/journal.pone.0157276 (2016).

17 Eleuteri, B., Aranda, S. & Ernfors, P. NoRC Recruitment by H2A.X Deposition at rRNA Gene Promoter Limits Embryonic Stem Cell Proliferation. *Cell reports* **23**, 1853-1866, doi:10.1016/j.celrep.2018.04.023 (2018).

18 Corsini, N. S. *et al.* Coordinated Control of mRNA and rRNA Processing Controls Embryonic Stem Cell Pluripotency and Differentiation. *Cell Stem Cell* **22**, 543-558 e512, doi:10.1016/j.stem.2018.03.002 (2018).
19 Kwon, S. C. *et al.* The RNA-binding protein repertoire of embryonic stem cells. *Nat Struct Mol Biol* **20**, 1122-1130, doi:10.1038/nsmb.2638 (2013).
20 Watanabe-Susaki, K. *et al.* Biosynthesis of ribosomal RNA in nucleoli regulates pluripotency and differentiation ability of pluripotent stem cells. *Stem Cells* **32**, 3099-3111, doi:10.1002/stem.1825 (2014).
21 Yang, A. *et al.* Nucleolin maintains embryonic stem cell self-renewal by suppression of p53 protein-dependent pathway. *J Biol Chem* **286**, 43370-43382, doi:10.1074/jbc.M111.225185 (2011).
22 You, K. T., Park, J. & Kim, V. N. Role of the small subunit processome in the maintenance of pluripotent stem cells. *Genes Dev* **29**, 2004-2009, doi:10.1101/gad.267112.115 (2015).
23 Cormier, S. *et al.* The murine ortholog of notchless, a direct regulator of the notch pathway in Drosophila melanogaster, is essential for survival of inner cell mass cells. *Mol Cell Biol* **26**, 3541-3549, doi:10.1128/MCB.26.9.3541-3549.2006 (2006).
24 Gayraud-Morel, B., Le Bouteiller, M., Commere, P. H., Cohen-Tannoudji, M. & Tajbakhsh, S. Notchless defines a stage-specific requirement for ribosome biogenesis during lineage progression in adult skeletal myogenesis. *Development* **145**, doi:10.1242/dev.162636 (2018).
25 Le Bouteiller, M. *et al.* Notchless-dependent ribosome synthesis is required for the maintenance of adult hematopoietic stem cells. *J Exp Med* **210**, 2351-2369, doi:10.1084/jem.20122019 (2013).
26 Han, H. *et al.* MBNL proteins repress ES-cell-specific alternative splicing and reprogramming. *Nature* **498**, 241-245, doi:10.1038/nature12270 (2013).
27 Ozmadenci, D. *et al.* Netrin-1 regulates somatic cell reprogramming and pluripotency maintenance. *Nat Commun* **6**, 7398, doi:10.1038/ncomms8398 (2015).
28 Buganim, Y. *et al.* Single-cell expression analyses during cellular reprogramming reveal an early stochastic and a late hierarchic phase. *Cell* **150**, 1209-1222, doi:10.1016/j.cell.2012.08.023 (2012).
29 Guo, L. *et al.* Resolving Cell Fate Decisions during Somatic Cell Reprogramming by Single-Cell RNA-Seq. *Mol Cell* **73**, 815-829 e817, doi:10.1016/j.molcel.2019.01.042 (2019).
30 Chen, H. *et al.* Reinforcement of STAT3 activity reprogrammes human embryonic stem cells to naive-like pluripotency. *Nat Commun* **6**, 7095, doi:10.1038/ncomms8095 (2015).
31 Saveanu, C. *et al.* Sequential protein association with nascent 60S ribosomal particles. *Mol Cell Biol* **23**, 4449-4460 (2003).
32 Liang, X. *et al.* Structural snapshots of human pre-60S ribosomal particles before and after nuclear export. *Nat Commun* **11**, 3542, doi:10.1038/s41467-020-17237-x (2020).
33 Zhou, Y., Musalgaonkar, S., Johnson, A. W. & Taylor, D. W. Tightly-orchestrated rearrangements govern catalytic center assembly of the ribosome. *Nat Commun* **10**, 958, doi:10.1038/s41467-019-08880-0 (2019).
34 Shubina, M. Y. *et al.* The GAR domain integrates functions that are necessary for the proper localization of fibrillarin (FBL) inside eukaryotic cells. *PeerJ* **8**, e9029, doi:10.7717/peerj.9029 (2020).

35 De Los Angeles, A. *et al.* Hallmarks of pluripotency. *Nature* **525**, 469-478, doi:10.1038/nature15515 (2015).
36 Pinto, J. P. *et al.* StemChecker: a web-based tool to discover and explore stemness signatures in gene sets. *Nucleic Acids Res* **43**, W72-77, doi:10.1093/nar/gkv529 (2015).
37 Oki, S. *et al.* ChIP-Atlas: a data-mining suite powered by full integration of public ChIP-seq data. *EMBO Rep* **19**, doi:10.15252/embr.201846255 (2018).
38 Stefkova, K., Prochazkova, J. & Pachernik, J. Alkaline phosphatase in stem cells. *Stem Cells Int* **2015**, 628368, doi:10.1155/2015/628368 (2015).
39 Wobus, A. M., Guan, K., Yang, H. T. & Boheler, K. R. Embryonic stem cells as a model to study cardiac, skeletal muscle, and vascular smooth muscle cell differentiation. *Methods Mol Biol* **185**, 127-156, doi:10.1385/1-59259-241-4:127 (2002).
40 Frum, T. *et al.* Oct4 cell-autonomously promotes primitive endoderm development in the mouse blastocyst. *Developmental cell* **25**, 610-622, doi:10.1016/j.devcel.2013.05.004 (2013).
41 Radzisheuskaya, A. *et al.* A defined Oct4 level governs cell state transitions of pluripotency entry and differentiation into all embryonic lineages. *Nature cell biology* **15**, 579-590, doi:10.1038/ncb2742 (2013).
42 Kater, L. *et al.* Visualizing the Assembly Pathway of Nucleolar Pre-60S Ribosomes. *Cell* **171**, 1599-1610 e1514, doi:10.1016/j.cell.2017.11.039 (2017).
43 Chaker-Margot, M. & Klinge, S. Assembly and early maturation of large subunit precursors. *RNA* **25**, 465-471, doi:10.1261/rna.069799.118 (2019).
44 Kappel, L. *et al.* Rlp24 activates the AAA-ATPase Drg1 to initiate cytoplasmic pre-60S maturation. *The Journal of cell biology* **199**, 771-782, doi:10.1083/jcb.201205021 (2012).
45 Lo, K. Y. *et al.* Defining the pathway of cytoplasmic maturation of the 60S ribosomal subunit. *Mol Cell* **39**, 196-208, doi:10.1016/j.molcel.2010.06.018 (2010).
46 Tafforeau, L. *et al.* The complexity of human ribosome biogenesis revealed by systematic nucleolar screening of Pre-rRNA processing factors. *Mol Cell* **51**, 539-551, doi:10.1016/j.molcel.2013.08.011 (2013).
47 Weis, F. *et al.* Mechanism of eIF6 release from the nascent 60S ribosomal subunit. *Nat Struct Mol Biol* **22**, 914-919, doi:10.1038/nsmb.3112 (2015).
48 Gregory, B. *et al.* The small and large ribosomal subunits depend on each other for stability and accumulation. *Life Sci Alliance* **2**, doi:10.26508/lsa.201800150 (2019).
49 Rotenberg, M. O., Moritz, M. & Woolford, J. L., Jr. Depletion of Saccharomyces cerevisiae ribosomal protein L16 causes a decrease in 60S ribosomal subunits and formation of half-mer polyribosomes. *Genes Dev* **2**, 160-172, doi:10.1101/gad.2.2.160 (1988).
50 Zhao, Y., Sohn, J. H. & Warner, J. R. Autoregulation in the biosynthesis of ribosomes. *Mol Cell Biol* **23**, 699-707, doi:10.1128/mcb.23.2.699-707.2003 (2003).
51 Yi, Y. *et al.* A PRC2-independent function for EZH2 in regulating rRNA 2'-O methylation and IRES-dependent translation. *Nature cell biology* **23**, 341-354, doi:10.1038/s41556-021-00653-6 (2021).
52 Mills, E. W. & Green, R. Ribosomopathies: There's strength in numbers. *Science* **358**, doi:10.1126/science.aan2755 (2017).
53 Ingolia, N. T., Lareau, L. F. & Weissman, J. S. Ribosome profiling of mouse embryonic stem cells reveals the complexity and dynamics of mammalian proteomes. *Cell* **147**, 789-802, doi:10.1016/j.cell.2011.10.002 (2011).

54 Friend, K., Brooks, H. A., Propson, N. E., Thomson, J. A. & Kimble, J. Embryonic Stem Cell Growth Factors Regulate eIF2alpha Phosphorylation. *PLoS One* **10**, e0139076, doi:10.1371/journal.pone.0139076 (2015).
55 Carey, B. W., Markoulaki, S., Beard, C., Hanna, J. & Jaenisch, R. Single-gene transgenic mouse strains for reprogramming adult somatic cells. *Nat Methods* **7**, 56-59, doi:10.1038/nmeth.1410 (2010).
56 Moffat, J. *et al.* A lentiviral RNAi library for human and mouse genes applied to an arrayed viral high-content screen. *Cell* **124**, 1283-1298, doi:10.1016/j.cell.2006.01.040 (2006).
57 Rueden, C. T. *et al.* ImageJ2: ImageJ for the next generation of scientific image data. *BMC Bioinformatics* **18**, 529, doi:10.1186/s12859-017-1934-z (2017).
58 Madeira, F. *et al.* The EMBL-EBI search and sequence analysis tools APIs in 2019. *Nucleic Acids Res* **47**, W636-W641, doi:10.1093/nar/gkz268 (2019).
59 Waterhouse, A. M., Procter, J. B., Martin, D. M., Clamp, M. & Barton, G. J. Jalview Version 2--a multiple sequence alignment editor and analysis workbench. *Bioinformatics* **25**, 1189-1191, doi:10.1093/bioinformatics/btp033 (2009).
60 Bertoni, M., Kiefer, F., Biasini, M., Bordoli, L. & Schwede, T. Modeling protein quaternary structure of homo- and hetero-oligomers beyond binary interactions by homology. *Scientific reports* **7**, 10480, doi:10.1038/s41598-017-09654-8 (2017).
61 Bienert, S. *et al.* The SWISS-MODEL Repository-new features and functionality. *Nucleic Acids Res* **45**, D313-D319, doi:10.1093/nar/gkw1132 (2017).
62 Waterhouse, A. *et al.* SWISS-MODEL: homology modelling of protein structures and complexes. *Nucleic Acids Res* **46**, W296-W303, doi:10.1093/nar/gky427 (2018).
63 Wang, L., Wang, S. & Li, W. RSeQC: quality control of RNA-seq experiments. *Bioinformatics* **28**, 2184-2185, doi:10.1093/bioinformatics/bts356 (2012).
64 Soneson, C., Love, M. I. & Robinson, M. D. Differential analyses for RNA-seq: transcript-level estimates improve gene-level inferences. *F1000Res* **4**, 1521, doi:10.12688/f1000research.7563.2 (2015).
65 Love, M. I., Huber, W. & Anders, S. Moderated estimation of fold change and dispersion for RNA-seq data with DESeq2. *Genome Biol* **15**, 550, doi:10.1186/s13059-014-0550-8 (2014).
66 Maere, S., Heymans, K. & Kuiper, M. BiNGO: a Cytoscape plugin to assess overrepresentation of gene ontology categories in biological networks. *Bioinformatics* **21**, 3448-3449, doi:10.1093/bioinformatics/bti551 (2005).
67 Shannon, P. *et al.* Cytoscape: a software environment for integrated models of biomolecular interaction networks. *Genome Res* **13**, 2498-2504, doi:10.1101/gr.1239303 (2003).

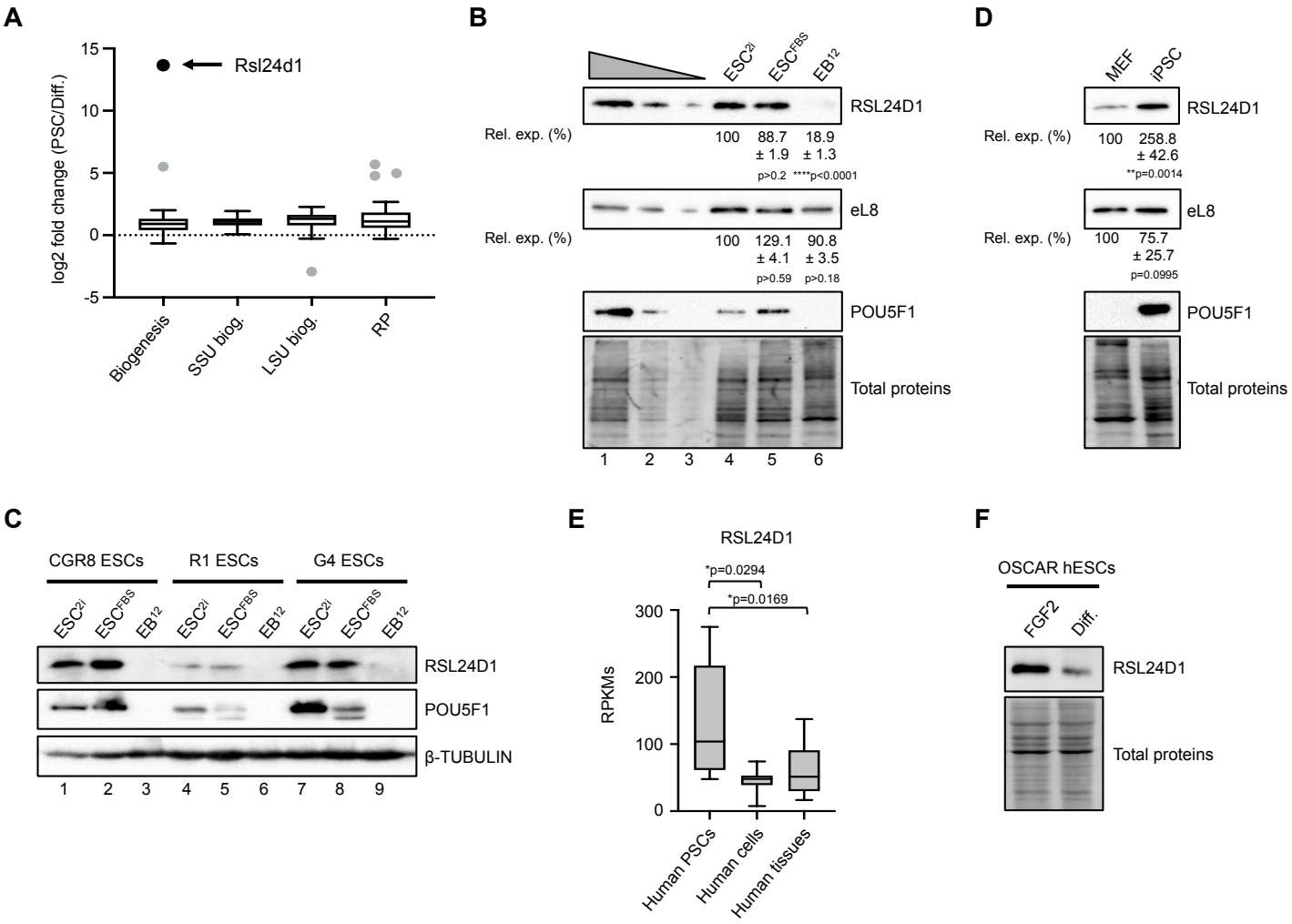

Fig. 1 Rsl24d1 expression is enriched in PSCs. (A) Box plot representation of mRNA expression changes in mouse PSCs (5 ESC lines and 2 iPSC clones) and 6 differentiated cell lines, measured by RNA-seq, for factors involved in common biogenesis steps (Biogenesis), specific biogenesis factors of the 40S (SSU biog.) or of the 60S subunits (LSU biog.), and ribosomal proteins (RP). Outlier values are represented by individual grey circles and Rsl24d1 is indicated by a black circle. Additional details are provided in Figure S1A and in Table S1. (B) Representative immunoblot of mouse CGR8 ESCs cultivated in ESC^{2i} or ESC^{FBS} conditions or differentiated in embryoid bodies for 12 days (EB^{12}) (n=4). Lanes 1 to 3 correspond to serial of dilutions of ESC^{FBS} (1:1, 1:3 and 1:9, respectively). TCE labeling of tryptophan-containing proteins (Total Proteins) is used for normalization. Quantifications of RSL24D1 and RPL8 signals normalized to total proteins and relative to the ESC^{2i} condition (Rel. exp. (%)) are indicated. Paired two-tailed Student's t-test.
(C) Representative immunoblot of 3 unrelated mouse ESC lines (CGR8, R1 and G4) cultivated in ESC^{2i}, ESC^{FBS} and differentiated (EB^{12}) conditions, as in panel B. β-TUBULIN levels are shown as a loading control. (D) Representative immunoblot of MEFs and in iPSCs reprogrammed from MEFs derived from $R26^{rtTA}$;$Col1a1^{4F2A}$ mice after ectopic expression of Pou5f1, Sox2, Klf4 and cMyc (n=4). TCE-labeled total proteins are used for normalization. Quantifications of immunoblot signals normalized to total proteins and relative to the "MEF" conditions (Rel. exp. (%)) are indicated. Paired two-tailed Student's t-test. (E) Box plot representation of normalized RSL24D1 mRNA levels in RPKMs (Reads per kilo base per million mapped reads) across 5 human PSC models, 7 human cell lines and 16 adult tissues based on published RNA-seq profiles (36). Unpaired two-tailed Student's t-test. (F) Representative immunoblot of human OSCAR ESCs maintained in pluripotent state in the presence of FGF2 or *in vitro* differentiated into EBs (Diff.). TCE-labeled total proteins are used as a loading control (n=3).

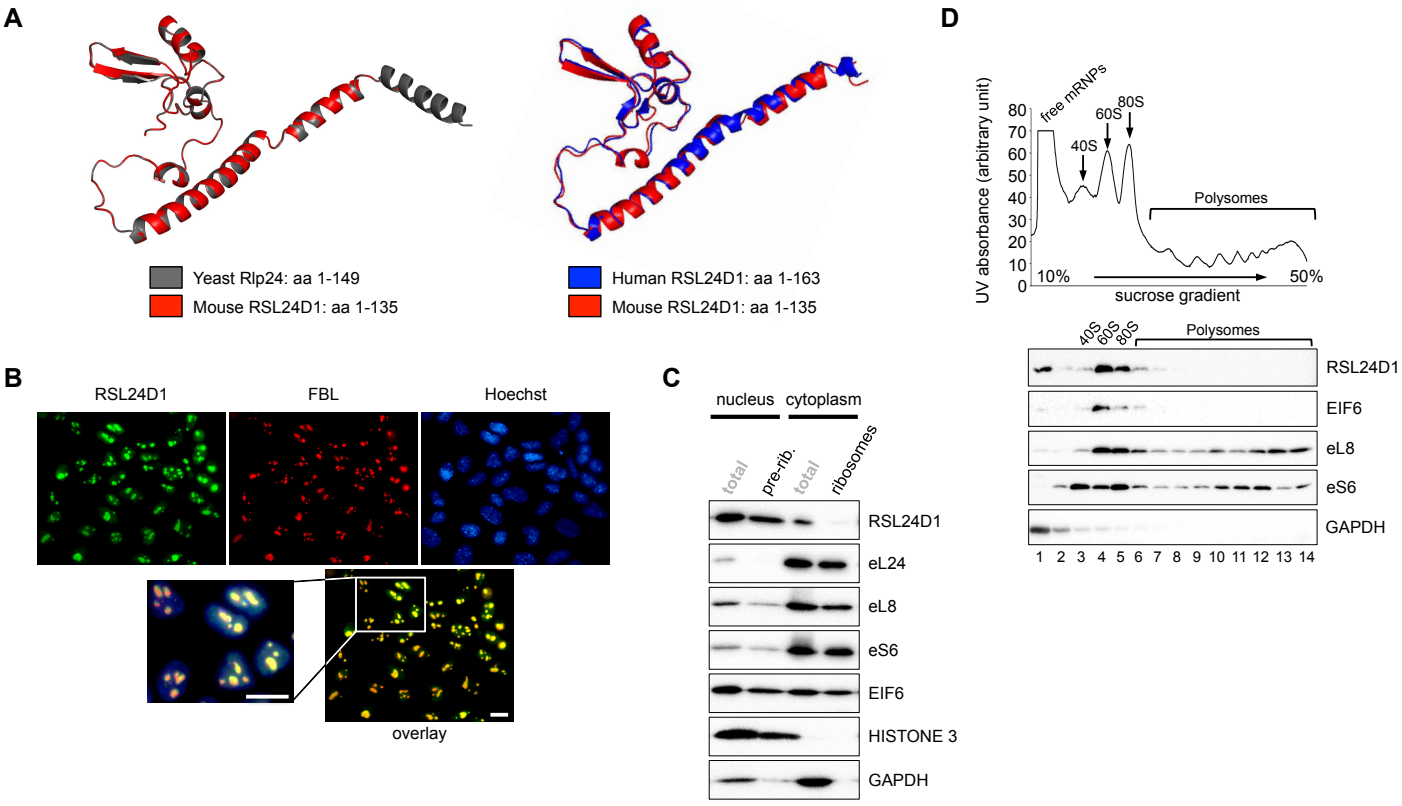

Fig. 2 RSL24D1 protein is associated with pre-60S subunits in mouse ESCs. (A) Comparison of the mouse RSL24D1 predicted structure (amino acids 1-135, red colour) with the yeast Rlp24 structure (amino acids 1-149, grey colour, left panel) and the human RSL24D1 structure (amino acids 1-163, blue colour, right panel) (Liang et al, 2020; Zhou et al, 2019). The mouse RSL24D1 protein structure was predicted from the 6N8J and 6LSS PDB structures using the swiss-model structure assessment tool (Waterhouse et al, 2018). (B) Representative images of naive CGR8 cells stained with Hoechst and with anti-FBL and anti-RSL24D1 antibodies (20X objective). (C) Representative immunoblots of ESC^{FBS} nucleo-cytoplasmic fractions before (total) and after sucrose cushion purifications of nuclear pre-ribosomes (pre-rib.) and cytoplasmic ribosomes (ribosomes). HISTONE 3 and GAPDH are shown as specific nuclear and cytoplasmic proteins, respectively. (D) Polysome profiling of CGR8 ESC^{FBS} cytoplasmic extracts. Ribosome-free fractions (free mRNPs), 40S, 60S, 80S monosomes and polysomes are detected by UV-absorbance and indicated on the absorbance curve (upper panel). Representative immunoblots of gradient fractions (lower panel). GAPDH is used as a control of the free mRNPs.

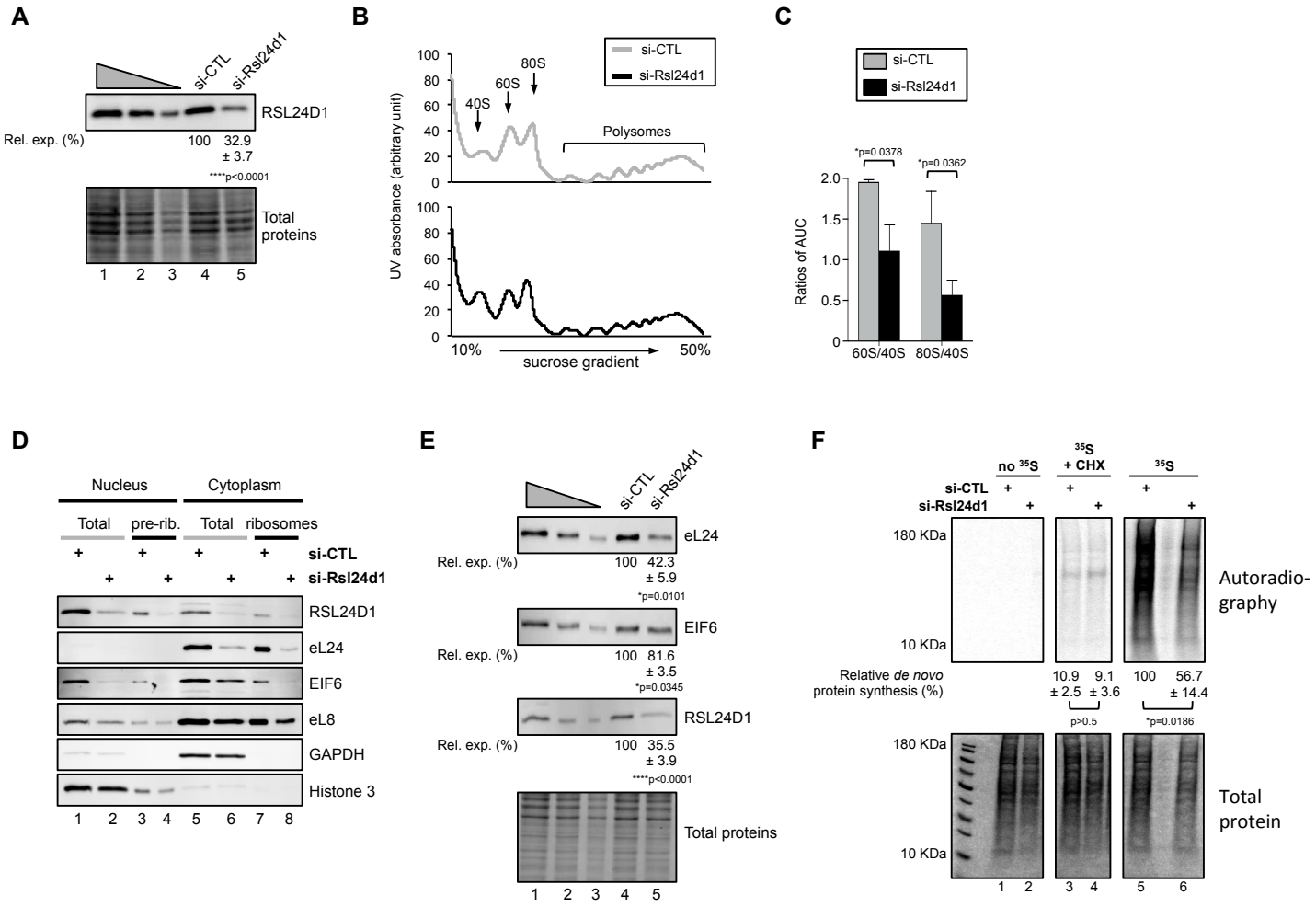

Fig. 3 RSL24D1 depletion alters ribosome biogenesis and protein translation. (A) Representative immunoblot of total extracts from si-CTL and si-Rsl24d1 treated CGR8 ESC^{FBS}. Lanes 1 to 3 correspond to serial dilutions of ESC^{FBS} (1:1, 1:3 and 1:9, respectively). TCE-labeled total proteins are used for normalization. Quantifications of RSL24D1 signals normalized to total proteins and relative to the si-CTL-treated conditions (Rel. exp. (%)) are indicated. Unpaired two-tailed Student's t test. (B) Polysome profiling of cytoplasmic extracts from CGR8 ESC^{FBS} treated with non-targeting siRNAs (grey color) or siRNAs targeting Rsl24d1 (black color). 40S, 60S, 80S and polysomes are detected by UV-absorbance and indicated on the absorbance curve.

(C) Histograms indicating ratios of 60S/40S and 80S/40S absorbance peaks calculated by determining the area under the curve (AUC) for the 40S, 60S and 80S absorbance signals (n=3). Unpaired two-tailed Student's t test. (D) Representative immunoblot of nucleo-cytoplasmic fractions of CGR8 ESC^{FBS} transfected with non-targeting (si-CTL) or Rsl24d1-targeting siRNAs, before (Total) and after ribosome purifications on sucrose cushions (pre-rib. and ribosomes). HISTONE 3 and GAPDH are shown as specific nuclear and cytoplasmic proteins, respectively. (E) Representative immunoblots of total extracts from si-CTL and si-Rsl24d1 treated CGR8 ESC^{FBS} (n=3). Lanes 1 to 3 correspond to serial dilutions of si-CTL-treated ESC^{FBS} (1:1, 1:3 and 1:9, respectively). TCE-labeled total proteins are used for normalization. Quantifications of immunoblot signals normalized to total proteins and relative to the si-CTL-treated condition (Rel. exp. (%)) are indicated. Unpaired two-tailed Student's t test. (F) Representative autoradiography (upper panel) and coomassie staining (lower panel) of SDS-PAGE of total extracts from si-CTL and si-Rsl24d1 treated CGR8 ESC^{FBS}, in the presence or absence of Cycloheximide (CHX) and ^{35}S-labelled methionine and cysteine. Quantifications of ^{35}S signals (autoradiography) are normalized to total proteins (coomassie staining) and expressed relative to si-CTL- and ^{35}S-methionine-treated ESC^{FBS} (n=3). Unpaired two-tailed Student's t test.

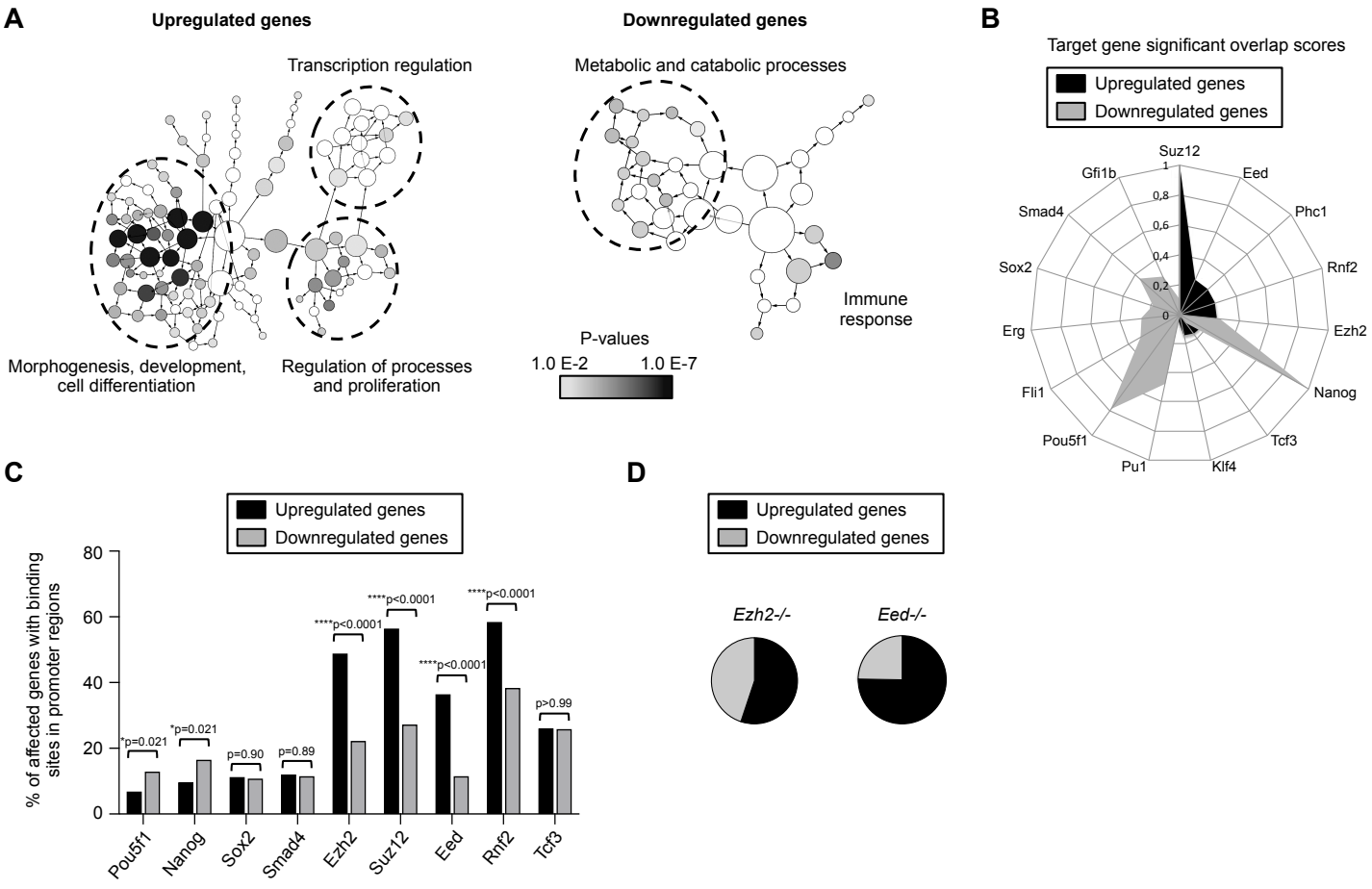

Fig. 4 RSL24D1 is required to maintain the regulation of pluripotency and differentiation transcriptional programs. (A) Gene ontology (GO) enrichment analysis of biological process terms associated with genes differentially expressed in CGR8 cells treated with Rsl24d1 siRNAs. The left and right panels represent hierarchical trees of the most enriched terms for genes up- or downregulated in Rsl24d1-depleted cells, respectively. The size of the nodes represents the numbers of genes associated to each GO term, and the corresponding p-values are indicated by colour codes. The most represented GO term categories are indicated. The corresponding data are available in Table S3. (B) Radar plot summarizing the Stemchecker analysis for PTFs and chromatin-associated factors with a significant association score to the 250 upregulated and the 259 downregulated genes in Rsl24d1-depleted ESC^{FBS} CGR8 cells. The corresponding data are available in Table S4. (C) Diagram showing the relative proportion of up- and downregulated genes in Rsl24d1-depleted CGR8 cells that contain binding sites in their promoter region (± 1kb from transcription start sites or TSS) for indicated transcription and chromatin-associated factors, established by ChIP-seq analyses (52). Fisher exact test. (D) Analysis of the proportion of genes displaying similar expression changes, either up- or downregulation, in Rsl24d1-depleted CGR8 cells and in *Eed*$^{-/-}$ or *Ezh2*$^{-/-}$ ESCs (7-8).

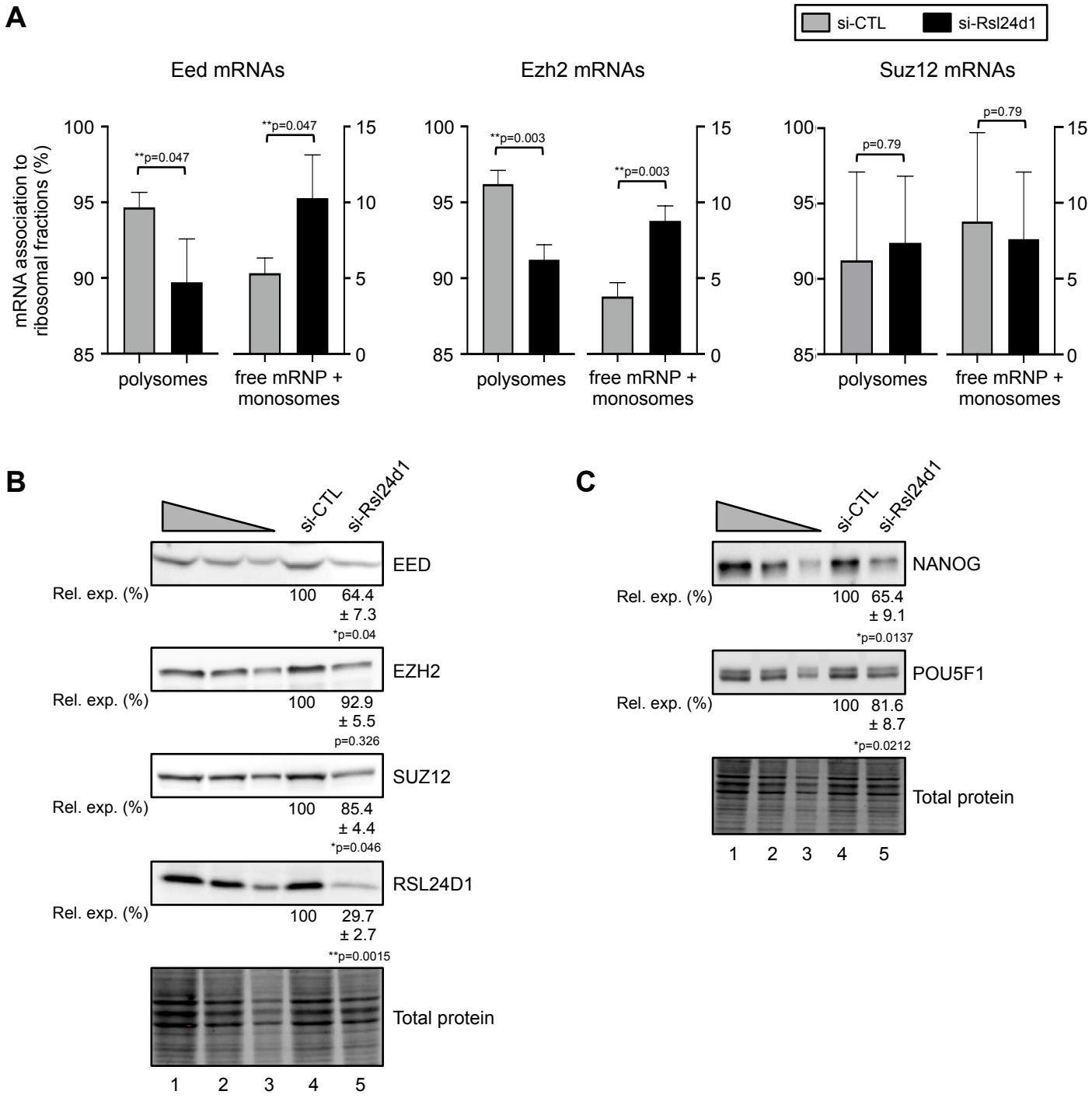

Fig. 5 RSL24D1 depletion impairs the translation of core PRC2 factors and the expression of key PTFs. (A) Relative proportions of Eed, Ezh2 and Suz12 mRNAs detected by qRT-PCR in free mRNPs, monosomal or polysomal fractions, based on quantifications detailed in the supplementary Figure S5C, in si-CTL (grey) or si-Rsl24d1 (black) treated CGR8 ESC^{FBS} (n=3). Paired two-tailed Student's t-test. (B) Representative immunoblots of RSL24D1 (n=3), EED (n=3), EZH2 (n=3) and SUZ12 (n=4) in si-CTL or si-Rsl24d1 treated CGR8 ESC^{FBS}. Lanes 1 to 3 correspond to serial dilutions of si-CTL-treated ESC^{FBS} (1:1, 1:3 and 1:9, respectively). TCE-labeled total proteins are used for normalization. Quantifications of immunoblot signals normalized to total proteins and relative to the si-CTL-treated conditions (Rel. exp. (%)) are indicated. Paired two-tailed Student's t-test. (C) As previously described for panel B for POU5F1 (n=3) and NANOG (n=3) si-CTL or si-Rsl24d1 treated CGR8 ESC^{FBS}. Paired two-tailed Student's t-test.

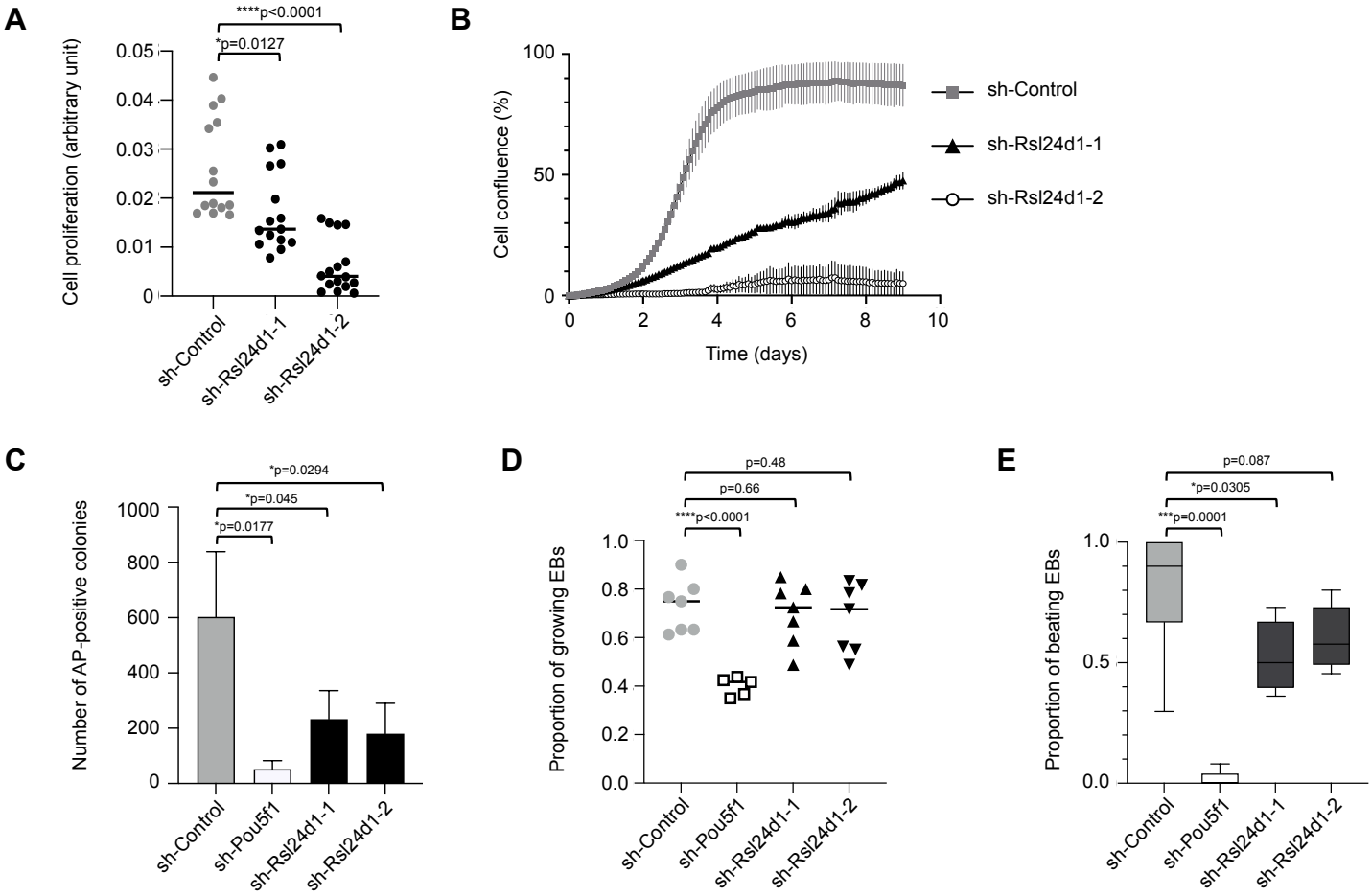

Fig. 6 RSL24D1 is required for mouse ESC proliferation and self-renewal. (A) Analysis of proliferative capacities defined by the cell growth index quantified by the xCELLigence RTCA technology in the first 12 hours after plating CGR8 cells in ESC^{FBS} conditions. Cells were infected with lentiviral vectors expressing a control non-targeting shRNA (grey dots, sh-Control, n=14 wells), sh-Rsl24d1-1 (black dots, n=15 wells) or sh-Rsl24d1-2 (black dots, n=16 wells). Unpaired two-tailed Student's t test. (B) Long term proliferation estimated by cell confluency analysis of CGR8 ESC^{FBS} expressing sh-Control (grey squares), sh-Rsl24d1-1 (black triangles) or sh-Rsl24d1-2, (white circles) shRNAs (n=6). (C) Analysis of the self-renewing capacities of CGR8 ESC^{FBS} estimated by the quantification of individual colonies with alkaline phosphatase activity detected by colorimetric labelling (corresponding data are detailed in Supplementary Fig. 6C). Colonies expressing control- (n=4), Pou5f1- (n=4) or Rsl24d1-targeting shRNAs (sh-Rsl24d1-1, sh-Rsl24d1-2) (n=5) were compared. Unpaired two-tailed Student's t test. (D) Analysis of *in vitro* differentiation capacities of CGR8 cells expressing control- (n=7), Pou5f1- (n=5) or Rsl24d1-shRNAs (n=7) defined by the proportion of embryoid bodies surviving and growing during a 12-day differentiation course. Unpaired two-tailed Student's t test. (E) Analysis of the proportion of 12-day old EBs, generated from CGR8 cells expressing control- (n=7), Pou5f1- (n=5) or Rsl24d1-shRNAs (n=7), containing functional self-beating cardiomyocytes. Unpaired two-tailed Student's t test.

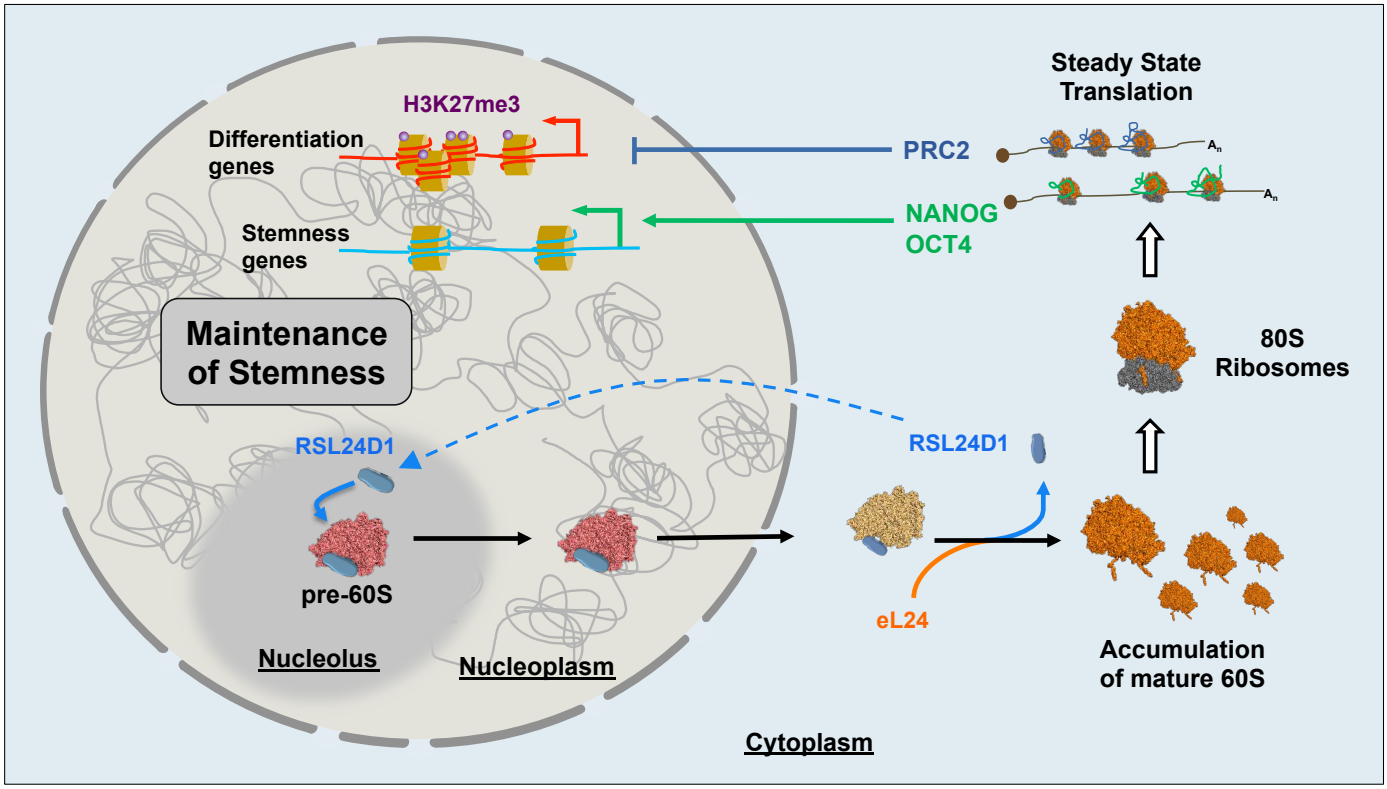

Fig. 7 Model describing the functions of RSL24D1 in the LSU biogenesis and in the translational regulation of key pluripotency and developmental programs in mouse ESCs.

Supplementary Files

This is a list of supplementary files associated with this preprint. Click to download.

- SupplementalTableS1.xlsx
- SupplementalTableS2.xlsx
- SupplementalTableS3.xlsx
- SupplementalTableS4.xlsx
- SupplementalTableS5.xlsx
- SupplementalTableS6.xlsx
- supplementaryfigures.pdf